

Quantum Zeno stabilization in weak continuous measurement of two qubits

Rusko Ruskov,^{1*} Alexander N. Korotkov,² and Ari Mizel¹

¹*Department of Physics and Materials Research Institute,*

Penn State University, University Park, Pennsylvania 16802, U.S.A.

²*Department of Electrical Engineering, University of California, Riverside, CA 92521-0204, U.S.A.*

(Dated: October 31, 2018)

We have studied quantum coherent oscillations of two qubits under continuous measurement by a symmetrically coupled mesoscopic detector. The analysis is based on a Bayesian formalism that is applicable to individual quantum systems. Measurement continuously collapses the two-qubit system to one of the sub-spaces of the Bell basis. For a detector with linear response this corresponds to measurement of the total spin of the qubits. In the other extreme of purely quadratic response the operator $\sigma_y^1 \sigma_y^2 + \sigma_z^1 \sigma_z^2$ is measured. In both cases, collapse naturally leads to spontaneous entanglement which can be identified by measurement of the power spectrum and/or the average current of the detector. Asymmetry between the two qubits results in evolution between the different measurement subspaces. However, when the qubits are even weakly coupled to the detector, a kind of quantum Zeno effect cancels the gradual evolution and replaces it with rare, abrupt switching events. We obtain the asymptotic switching rates for these events and confirm them with numerical simulations. We show how such switching affects the observable power spectrum on different time scales.

PACS numbers: 73.23.-b; 03.65.Ta; 03.65.Xp; 03.67.Lx

I. INTRODUCTION

The quantum Zeno effect is an intriguing prediction that arises in the context of quantum measurement theory.^{1,2,3} It states that a sequence of strong orthodox measurements can “freeze” a system in its quantum state, so that in the Zeno limit of very frequent measurements, the system is prevented from decay and/or subsequent evolution. Since its original formulation,^{4,5} there has been continued theoretical development^{6,7,8,9} as well as experimental demonstration^{12,13} in an ensemble of quantum micro systems – trapped ions (or atoms) probed via fast (strong) quantum-optical measurements.

With the recent experimental advances in the deliberate fabrication of two-level quantum systems, such as superconducting qubits¹⁴ or double quantum dots¹⁵ (DQD), it has become possible to perform experiments on *individual* quantum systems (see, e.g., Refs. 26,16). However, it can be very difficult to make repeated strong orthodox measurements on such systems. Instead, a more practical measurement scheme utilizes a detector such as a quantum point contact¹⁵ (QPC) or a single-electron transistor¹⁷ (SET) that is weakly coupled to the qubit(s). The measurement record in such a situation is a fluctuating current $I(t)$ that accumulates a distinguishable signal-to-noise ratio after some time.^{17,18}

On one hand, the weak coupling between detector and qubit(s) permits the quantum system to remain relatively well isolated from “outside” classical noise. On the other hand, it means that instead of simple abrupt collapse,¹⁹ we have to deal with a theory of continuous (weak) mea-

surements of a single quantum system. The development of such theories started long ago^{20,21,22} and has attracted most attention in quantum optics.^{23,24,25} Despite the similarity of their underlying principles, the theories may differ significantly in formalism and area of application; for solid-state qubits a “Bayesian” theory was developed relatively recently.²⁶ This formalism is reviewed in Ref. 27, and its equivalence to the quantum trajectory approach translated^{28,29} from quantum optics is shown in Ref. 28.

For single-qubit continuous measurement,^{30,31} it was shown that in a hypothetical situation of *very strong* continuous qubit-detector coupling, it would be possible to approach the quantum Zeno limit. For large (but finite) qubit-detector coupling long periods of “freezing” of the single-qubit state are interrupted by rare, abrupt jumps between qubit states. Such jumps produce corresponding jumps in the average detector current signal that closely follows the qubit evolution. This is in agreement with the classical character of the strong coupling measurement regime.^{30,32,33}

In this paper we show that the Zeno-like regime can arise even in a relatively practical *weak* continuous measurement context. We initially consider two identical qubits coupled symmetrically to a detector. Measurement continuously collapses the two-qubit state into *measurement subspaces*, i.e., stable “points” or stable multi-dimensional subspaces of the two-qubit Hilbert space. On a time scale greater than the characteristic measurement time the collapse is like a projective measurement in the Bell basis. For a detector with linear or non-linear response³⁴ this corresponds to measurement of the total “spin” of the qubits $(\vec{\sigma}^{(1)} + \vec{\sigma}^{(2)})^2$. In the degenerate case of purely quadratic detection³⁵ the spin-1 subspace itself splits and effectively the operator $\sigma_y^{(1)} \sigma_y^{(2)} + \sigma_z^{(1)} \sigma_z^{(2)}$ is measured. The Zeno-like regime manifests itself in

*On leave of absence from Institute for Nuclear Research and Nuclear Energy, Sofia BG-1784, Bulgaria

a situation of slightly asymmetric qubits, wherein the Hamiltonian attempts to evolve a collapsed state out of its measurement subspace. Our results show that measurement stabilizes the state, stifling this evolution. Instead of gradual evolution, one finds rare quantum switching events between different subspaces.

Given the noisy experimental signal $I(t)$, such switching events can be identified by consideration of the power spectrum and/or average current. Using the stochastic Bayesian approach we evaluate the power spectrum in several important cases including the linear and purely quadratic detection regimes. We estimate the measurement time needed to accumulate the spectrum and show that even for a non-ideal detector it is possible to observe switching events if the lifetime of the subspaces is large enough. On a long time scale compared to the subspace's lifetime, the switching events lead to an averaging of the power spectrum (effective decreasing of the spectral peaks) and also may produce a telegraph noise peak near zero frequency. The resulting long-time-average power spectrum is in accordance with both numerical simulation of the spectrum through Bayesian equations³⁴ and with the ensemble averaged approach.^{35,36}

As expected in the quantum Zeno effect, the state “survival probability” evaluated from quantum master equations decays quadratically in time^{4,5,6} for small times and exponentially for times⁷ that are sufficiently large compared to the measurement time. We have obtained analytically the corresponding “lifetimes” of the subspaces for small deviations from the symmetric situation. We have verified our results by Monte Carlo simulations of the measurement process.

The presentation of our results is organized as follows. In Sec. II, we review the Hamiltonian and the Bayesian equations of motion for weak continuous measurements of a two-qubit system. Sec. III describes in detail the measurement collapse scenarios that result from the Bayesian equations. In Sec. IV, the quantum Zeno effect is demonstrated when the two qubits are asymmetrical. Sec. V presents conclusions.

II. MODEL HAMILTONIAN AND BAYESIAN EQUATIONS OF MOTION

A. Model Hamiltonian

Fig. 1(a) shows possible realization of the setup that we analyze. Each qubit is made of a double quantum dot¹⁵ (DQD), occupied by a single electron, while the detector is a quantum point contact (QPC) located in between DQDs. Another possible realization (not shown) is based on single-Cooper-pair-box (SCPB) qubits¹⁴ measured by a single-electron transistor (SET).

In the Hamiltonian of the system,

$$\mathcal{H} = \mathcal{H}_{QB} + \mathcal{H}_{DET} + \mathcal{H}_{INT}, \quad (1)$$

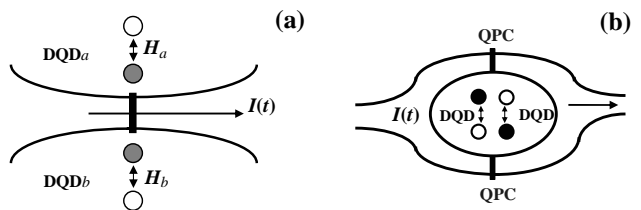


FIG. 1: Schematic of two qubits measured by a linear and non-linear detector. (a): Realization based on double quantum dots measured by a QPC. (b): Possible realization of a purely quadratic detector based on double quantum dots measured by two QPCs.

the first term describes two qubits alone with direct interaction between them,

$$\begin{aligned} \mathcal{H}_{QB} = & (\varepsilon_a/2)(a_\downarrow^\dagger a_\downarrow - a_\uparrow^\dagger a_\uparrow) + H_a(a_\uparrow^\dagger a_\downarrow + a_\downarrow^\dagger a_\uparrow) \\ & + (\varepsilon_b/2)(b_\downarrow^\dagger b_\downarrow - b_\uparrow^\dagger b_\uparrow) + H_b(b_\uparrow^\dagger b_\downarrow + b_\downarrow^\dagger b_\uparrow) \\ & + U(a_\uparrow^\dagger a_\uparrow - a_\downarrow^\dagger a_\downarrow)(b_\uparrow^\dagger b_\uparrow - b_\downarrow^\dagger b_\downarrow) \end{aligned} \quad (2)$$

The amplitudes H_a and H_b describe tunneling within each qubit while ε_a and ε_b are the energy biases of each qubit. In the realization shown in Fig. 1(a), U gives the strength of the Coulomb interaction. For other realizations, the interaction may arise from a different physical source. In the absence of interaction ($U = 0$), each qubit becomes an independent two level system. The free Rabi oscillation frequencies of qubits “a” and “b” are then given by $\tilde{\Omega}_a \equiv (4H_a^2 + \varepsilon_a^2)^{1/2}/\hbar$ and $\tilde{\Omega}_b \equiv (4H_b^2 + \varepsilon_b^2)^{1/2}/\hbar$ respectively. In the following it will be convenient to define the Rabi frequencies at zero energy bias $\Omega_a \equiv 2H_a/\hbar$ and $\Omega_b \equiv 2H_b/\hbar$.

As an example of a detector we consider the case³⁷ of a low transparency QPC, with Hamiltonian

$$\mathcal{H}_{DET} = \sum_l E_l c_l^\dagger c_l + \sum_r E_r c_r^\dagger c_r + \sum_{l,r} (T c_r^\dagger c_l + \text{H.c.}) \quad (3)$$

An operator of the form c_l^\dagger (c_r^\dagger) creates an electron in the left (right) lead of the detector. The final term causes electrons to make transitions between the leads. We sum over all states l in the left lead and all states r in the right lead. The qubit–detector interaction term can be written as

$$\begin{aligned} \mathcal{H}_{INT} = & \sum_{l,r} (a_\uparrow^\dagger a_\uparrow - a_\downarrow^\dagger a_\downarrow)(b_\uparrow^\dagger b_\uparrow - b_\downarrow^\dagger b_\downarrow) \chi c_r^\dagger c_l + \text{H.c.} \\ & + \sum_{l,r} (a_\uparrow^\dagger a_\uparrow - a_\downarrow^\dagger a_\downarrow) \Delta T_a c_r^\dagger c_l + \text{H.c.} \\ & + \sum_{l,r} (b_\uparrow^\dagger b_\uparrow - b_\downarrow^\dagger b_\downarrow) \Delta T_b c_r^\dagger c_l + \text{H.c.} \end{aligned} \quad (4)$$

The amplitudes T and ΔT_a , ΔT_b , χ are assumed independent of the energy of the tunneling electrons. For simplicity, we will consider a situation when there is no

relative phase between these amplitudes. Such a relative phase would lead to additional decoherence.^{40,41,42} From the form of (4), one sees that the detector's measurement basis is $|\uparrow\rangle, |\downarrow\rangle$ for each qubit. Eq. (4) is the most general detector-system interaction in this basis in the case of two qubits.³⁵ Higher terms in Eq. (4) will appear for larger number of qubits.

Purely quadratic detectors ($\chi \neq 0$ and $\Delta T_{a,b} = 0$) may be of use to perform simple quantum error correction protocols.³⁸ To realize such a detector physically, one possibility is to form two identical QPCs into two arms of an Aharonov-Bohm type loop (no magnetic field is applied). If two qubits are placed exactly at the geometrically symmetric point of the loop as in Fig. 1(b), we have a purely quadratic detector which responds only on the relative state of the two qubits, i.e. it does not distinguish between states $|\uparrow_a\uparrow_b\rangle$ and $|\downarrow_a\downarrow_b\rangle$ and also does not distinguish between $|\uparrow_a\downarrow_b\rangle$ and $|\downarrow_a\uparrow_b\rangle$. Ref. 36 presented an explicit example of a non-linear detector constructed to measure flux qubits in the form of a superconducting loop interrupted by two Josephson junctions.

The four basis states of two qubits, $|1\rangle \equiv |\uparrow_a\uparrow_b\rangle$, $|2\rangle \equiv |\uparrow_a\downarrow_b\rangle$, $|3\rangle \equiv |\downarrow_a\uparrow_b\rangle$, $|4\rangle \equiv |\downarrow_a\downarrow_b\rangle$, correspond to four values of the average current through the detector:

$$\begin{aligned} I_{1,2} &= 2\pi(T \pm \chi + \Delta T_a \pm \Delta T_b)^2 \rho_l \rho_r e^2 V / \hbar \\ I_{3,4} &= 2\pi(T \mp \chi - \Delta T_a \pm \Delta T_b)^2 \rho_l \rho_r e^2 V / \hbar, \end{aligned} \quad (5)$$

where V is the QPC voltage and ρ_l and ρ_r are the densities of states in the left and right leads.

Note that if a very large voltage were applied to the QPC for a short time, the current variances would become much smaller than the corresponding current differences. This is probably experimentally impractical, but in principle it would constitute a strong orthodox measurement.

B. Weak continuous measurements of qubits

In the course of a measurement, our knowledge about a quantum system is updated according to the result of the measurement. In the case of strong instantaneous measurements the update (“collapse”) is also instantaneous.¹⁹ In a weak continuous measurement, the change of the system's quantum state occurs gradually.²⁶ The measured result is intrinsically noisy (it is a noisy quasi-continuous current $I(t)$ or voltage $V(t)$ in the simplest solid-state realizations), so that the information from the detector is also acquired only gradually in time.

Quantitatively, such a random measurement process can be described by Bayesian equations²⁶ for the system density matrix $\rho_{ij}(t)$ that take into account the actual measurement result $I(t)$. For a system of qubits measured by a common detector they can be written^{39,40} as stochastic equations (in Itô form⁴³):

$$\dot{\rho}_{ij} = [I(t) - \sum_k \rho_{kk} I_k] \left(I_i + I_j - 2 \sum_k \rho_{kk} I_k \right) \frac{\rho_{ij}}{S_0}$$

$$- \left[\frac{(I_i - I_j)^2}{4S_0} + \gamma_{ij} \right] \rho_{ij} - \frac{i}{\hbar} [\mathcal{H}_{QB}, \rho]_{ij}, \quad (6)$$

where the summation is performed over all of the states of the system, the I_k are the corresponding current levels, S_0 gives the background low-frequency noise in the detector, and γ_{ij} is the decoherence rate. For a 2-qubit system, there are $2^2 = 4$ states in the sum over k and the I_k are given by (5). Eq. (6) assumes that the detector is functioning in a weakly responding regime: $|I_i - I_j| \ll I_i, I_j$; this justifies the use of a single low frequency noise S_0 for all states $|k\rangle$ of the system.

Eq. (6) can be obtained by a general “informational” Bayesian approach^{26,39,40} (see also an analogous derivation of the Bayesian equations for the measurement of a nano-resonator⁴¹). Since QPC is an ideal detector with 100% quantum efficiency and no “phase asymmetry”, the evolution due to measurement basically reduces to the “quantum Bayes theorem.”⁴⁴ It says that at a sufficiently short time scale in which the evolution by \mathcal{H}_{QB} can be neglected: 1) evolution of the diagonal density matrix elements in the measurement basis coincides with evolution of classical probabilities described by usual Bayes formula and 2) the purity measure $\rho_{ij}/\sqrt{\rho_{ii}\rho_{jj}}$ stays constant. Such a derivation does not assume linearity of the measurement device, so it is also relevant for the general non-linear coupling of (4). Essentially, Eq. (6) describes the interplay between the “intrinsic” qubit evolution (Rabi oscillations) and the evolution due to measurement. It implicitly assumes that the internal detector dynamics of (3) and (4) is much faster than the qubit dynamics due to \mathcal{H}_{QB} and measurement. This is seen explicitly in another approach^{26,35} that leads to the same Eq. (6). It uses generalized Bloch equations that couple the qubit dynamics and the number n of electrons that have passed through the detector (for the one-qubit case see Ref. 37). One assumes that the typical detector decoherence time is much smaller than the characteristic electron tunneling time, $\hbar/eV \ll e/I_0$ so that coherences between different passages of electrons can be neglected.²⁶ In order for the current to be considered continuous, the characteristic electron tunneling time must be much less than the time scale of the qubit dynamics, $e/I_0 \ll 2\pi/\Omega$. Then, in the weakly responding regime, when individual tunneling events produce only a small change of the qubit state it is convenient to condition the evolution on the current $I(t)$. These conditions are sufficient for the stochastic process $\rho_{ij}(t)$ to be Markovian and make it possible to obtain equation (6).

To simulate individual realizations of the random measurement process, the noisy detector current $I(t)$ can be expressed as

$$I(t) = \xi(t) + \sum_k \rho_{kk} I_k, \quad (7)$$

where $\xi(t)$ represents white noise with spectral density S_0 . For a measurement with an ideal detector there are no individual qubit decoherences ($\gamma_{ij} = 0$). As a result, Eq. (6) leads to purification of the qubit state in the

course of continuous measurement even though the qubit undergoes random time evolution.²⁶

Averaging over different realizations of the measurement process $I(t)$ in Eq. (6) means total ignorance of the particular measurement result and is equivalent to ensemble averaging. The ensemble average of the qubit state does exhibit decoherence even for an ideal detector. Averaging in Eq. (6) is simply achieved by removing the noise term.⁴³ The result is the standard ensemble-averaged equations⁴⁵ with ensemble dephasing rates $\Gamma_{ij} = (I_i - I_j)^2/4S_0 + \gamma_{ij}$

$$\dot{\rho}_{ij} = -\Gamma_{ij} \rho_{ij} - \frac{i}{\hbar} [\mathcal{H}_{QB}, \rho]_{ij}. \quad (8)$$

We see that even in the case $\gamma_{ij} = 0$ the averaging has produced a decoherence rate $(I_i - I_j)^2/4S_0$ which is the quantum limited decoherence from an “ensemble averaged” point of view.^{26,16,46,47}

Individual qubit decoherence $\gamma_{ij} \neq 0$ will arise if the detector is not ideal and may be understood as partial ignorance of the measurement result.²⁶ The contribution to γ_{ij} is parameterized by the detector ideality or efficiency η ($0 \leq \eta \leq 1$)

$$\gamma_{ij} = (1/\eta - 1) \frac{(I_i - I_j)^2}{4S_0}. \quad (9)$$

The partial ignorance may arise due to extra output noise⁴⁰ or when the QPC detector has a finite temperature T .²⁶ For finite temperature, one takes into account the total current through the QPC, $I(t) = I_{\rightarrow}(t) - I_{\leftarrow}(t)$, but ignores information contained in the partial currents “to the right” and “to the left” in the detector. Correspondingly the quantum ideality (efficiency) is reduced down to^{26,48} $\eta = \tanh^2(eV/2T)$.⁴⁹ Notice that no mutual dephasing need be present between two states i, j if $I_i = I_j$. Indeed, in this case the detector cannot distinguish between the two states and therefore there is no (relative) information to be received and subsequently ignored. Then both γ_{ij} and Γ_{ij} vanish. Of course, additional qubit decoherence can arise due to individual coupling of qubits to the environment. The equation for γ_{ij} will then change as we will see in Sec. IV.

III. SYMMETRIC WEAK CONTINUOUS MEASUREMENTS OF TWO IDENTICAL QUBITS

In the quantum Zeno effect, measurement suppresses Hamiltonian evolution, repeatedly collapsing the system back to a given state. To understand how this suppression happens, it is essential to develop an understanding of the process of collapse. In this section, we consider symmetric weak continuous measurement of two identical qubits. In this case the system collapses into *measurement subspaces* that can be identified and characterized. We present a detailed analysis of the possible collapse

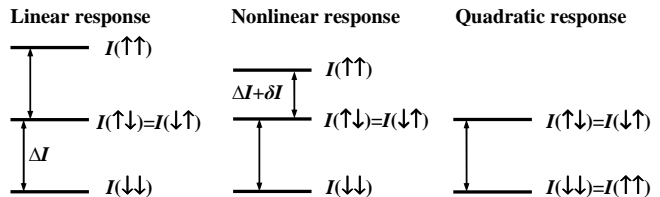


FIG. 2: Current levels for symmetrically coupled qubits, $\Delta I_a = \Delta I_b = \Delta I$. Linear, non-linear, and purely quadratic response.

scenarios for coupling to a linear, non-linear, or purely quadratic detection device. This sets the stage for the appearance of quantum Zeno physics in Sec. IV.

A. Preliminary view of dynamics

To consider solutions of (6), it is illuminating to analyze first the dynamics of the Hamiltonian (2) alone. Introducing the Bell basis proves convenient:

$$|1\rangle^B \equiv (|\uparrow_a \downarrow_b\rangle - |\downarrow_a \uparrow_b\rangle)/\sqrt{2}, \quad (10)$$

$$|2\rangle^B \equiv (|\uparrow_a \uparrow_b\rangle - |\downarrow_a \downarrow_b\rangle)/\sqrt{2}, \quad (11)$$

$$|3\rangle^B \equiv (|\uparrow_a \downarrow_b\rangle + |\downarrow_a \uparrow_b\rangle)/\sqrt{2}, \quad (12)$$

$$|4\rangle^B \equiv (|\uparrow_a \uparrow_b\rangle + |\downarrow_a \downarrow_b\rangle)/\sqrt{2}. \quad (13)$$

Using Eq. (2) it is straightforward to obtain the free evolution of the two qubits when the qubits are unbiased, $\varepsilon_a = \varepsilon_b = 0$, and do not interact, $U = 0$. In this case, the “+” and “-” subspaces of the Bell basis do not mix:

$$|1\rangle^B \rightarrow \cos(\Delta\Omega t/2) |1\rangle^B - i \sin(\Delta\Omega t/2) |2\rangle^B \quad (14)$$

$$|3\rangle^B \rightarrow \cos(\Omega t) |3\rangle^B - i \sin(\Omega t) |4\rangle^B, \quad (15)$$

where $\Delta\Omega \equiv \Omega_a - \Omega_b$ and $\Omega \equiv (\Omega_a + \Omega_b)/2$. This property persists when the direct interaction is switched on

$$|1\rangle^B \rightarrow [\cos(\Omega^- t) + i \frac{U}{\hbar\Omega^-} \sin(\Omega^- t)] |1\rangle^B \quad (16)$$

$$- i \frac{\Delta\Omega}{2\Omega^-} \sin(\Omega^- t) |2\rangle^B \quad (17)$$

$$|3\rangle^B \rightarrow [\cos(\Omega^+ t) + i \frac{U}{\hbar\Omega^+} \sin(\Omega^+ t)] |3\rangle^B$$

$$- i \frac{\Omega}{\Omega^+} \sin(\Omega^+ t) |4\rangle^B \quad (18)$$

$$\Omega^- \equiv \sqrt{(\Delta\Omega/2)^2 + (U/\hbar)^2} \quad (19)$$

$$\Omega^+ \equiv \sqrt{\Omega^2 + (U/\hbar)^2}. \quad (20)$$

Notice that $|1\rangle^B$ and $|2\rangle^B$ are eigenstates of \mathcal{H}_{QB} if $\Delta\Omega = \Omega_a - \Omega_b = 0$. When the energy biases $\varepsilon_a, \varepsilon_b$ are non-zero, there is no simple solution to the free equations of motion.

Turning to the coupling Hamiltonian (4), we note that our assumption of symmetric qubit couplings implies

$\Delta T_a = \Delta T_b$. In this case, two currents in (5) coincide, $I_2 = I_3 \equiv I_{23}$, as seen in Fig. 2, so the measurement cannot distinguish between the states $|2\rangle = |\uparrow_a \downarrow_b\rangle$ and $|3\rangle = |\downarrow_a \uparrow_b\rangle$. Qualitatively, the measurement alone tends to continuously collapse the system towards one of the subspaces with definite current. For a linear detector ($\chi = 0$ in Eq. (4)), there are three possible values of current I_1, I_4, I_{23} . Therefore, measurement collapses the system toward $|1\rangle$ or $|4\rangle$ or the subspace $\{|2\rangle, |3\rangle\}$. The current values are evenly spaced $I_1 - I_{23} = I_{23} - I_4$. For a non-linear detector ($\chi \neq 0$ in (4)), there are again three possible currents, so that measurement again collapses the system toward the same three subspaces. However, the currents are not evenly spaced. For a purely quadratic detector, ($\Delta T_{a,b} = 0$ in (4) while $\chi \neq 0$), $I_1 = I_4$ and $I_2 = I_3$, so the measurement itself collapses the system toward the subspace $\{|1\rangle, |4\rangle\}$ or toward the subspace $\{|2\rangle, |3\rangle\}$.

To describe the measurement process in more detail, it is convenient to introduce dimensionless qubit-detector couplings $C_a \equiv \hbar(\Delta I_a)^2/S_0 H_a$ and $C_b \equiv \hbar(\Delta I_b)^2/S_0 H_b$ where the current differences are defined as $\Delta I_a \equiv I_2 - I_4$, $\Delta I_b \equiv I_3 - I_4$, and $\Delta I \equiv (\Delta I_a + \Delta I_b)/2$; weak coupling corresponds to $C_a, C_b \lesssim 1$. To characterize the non-linearity of the detector, it is useful to define

$$\delta \equiv \frac{\delta I}{\Delta I} = \frac{[(I_1 - I_3) - (I_2 - I_4)]}{[(I_2 + I_3)/2 - I_4]}, \quad (21)$$

where $\delta I \equiv (I_1 - I_3) - (I_2 - I_4)$. These definitions apply in general to the non-symmetric coupling case; for identical symmetrically coupled qubits, $\Delta I_a = \Delta I_b = \Delta I$ and $C_a = C_b \equiv C$, and δI is indicated on Fig. 2. For linear coupling ($\chi = 0$) one has $\delta = 0$ while for the purely quadratic case $\delta = -2$.

B. Bayesian equations in the Bell basis

It is instructive to rewrite the Bayesian equations (6) in the Bell basis (10) - (13)

$$\frac{d\rho_{ij}^B}{dt} = \frac{d\rho_{ij}^B}{dt} \Big|_{meas} + \frac{d\rho_{ij}^B}{dt} \Big|_{H-evol}, \quad (22)$$

where we distinguish a non-unitary part due to measurement from a unitary part due to free Hamiltonian evolution. For qubits with identical couplings, these contributions (in Itô form) are:

$$\frac{d\rho_{ij}^B}{dt} \Big|_{meas} = \xi_{ij}\text{-term} - \frac{(\Delta I)^2}{\eta 4S_0} \times \begin{bmatrix} 0 & \rho_{12}^B & 0 & \rho_{14}^B \\ \cdot & \frac{\rho_{22}^B - \rho_{44}^B}{2} (2 + \delta)^2 & \rho_{23}^B & i \text{Im} \rho_{24}^B (2 + \delta)^2 \\ \cdot & \cdot & 0 & \rho_{34}^B \\ \cdot & \cdot & \cdot & \frac{\rho_{44}^B - \rho_{32}^B}{2} (2 + \delta)^2 \end{bmatrix} \quad (23)$$

$$+ (\delta + \frac{1}{2} \delta^2) \begin{bmatrix} 0 & \rho_{12}^B + \rho_{14}^B & 0 & \rho_{12}^B + \rho_{14}^B \\ \cdot & 0 & \rho_{23}^B + \rho_{43}^B & 0 \\ \cdot & \cdot & 0 & \rho_{32}^B + \rho_{34}^B \\ \cdot & \cdot & \cdot & 0 \end{bmatrix}.$$

The entries indicated with a dot are determined by the hermiticity of the matrices.

The noise term itself reads

$$\xi_{ij}\text{-term} = -\frac{2\Delta I}{S_0} \xi(t) \times \begin{bmatrix} \left(\begin{array}{cccc} z\rho_{11}^B & z\rho_{12}^B + \frac{\rho_{14}^B}{2} & z\rho_{13}^B & z\rho_{14}^B - \frac{\rho_{12}^B}{2} \\ \cdot & z(\rho_{22}^B - \frac{1}{2}) & z\rho_{23}^B - \frac{\rho_{43}^B}{2} & z\rho_{24}^B - \frac{\rho_{22}^B + \rho_{44}^B}{2} \\ \cdot & \cdot & z\rho_{33}^B & z\rho_{34}^B - \frac{\rho_{32}^B}{2} \\ \cdot & \cdot & \cdot & z(\rho_{44}^B - \frac{1}{2}) \end{array} \right) \\ -\frac{\delta}{4} \begin{bmatrix} 0 & \rho_{12}^B + \rho_{14}^B & 0 & \rho_{12}^B + \rho_{14}^B \\ \cdot & \rho_{22}^B - \rho_{44}^B & \rho_{23}^B + \rho_{43}^B & 2\rho_{24}^B + (\rho_{22}^B + \rho_{44}^B) \\ \cdot & \cdot & 0 & \rho_{32}^B + \rho_{34}^B \\ \cdot & \cdot & \cdot & -(\rho_{22}^B - \rho_{44}^B) \end{bmatrix} \end{bmatrix}, \quad (24)$$

where it proves convenient to introduce the quantity

$$z \equiv \rho_{11}(1 + \delta) - \rho_{44} = 2\text{Re} \rho_{24}^B \left(1 + \frac{\delta}{2}\right) + \frac{\delta}{2} (\rho_{22}^B + \rho_{44}^B) \quad (25)$$

given in the measurement basis and in the Bell basis. Since the detector signal (7) can be expressed, using (21) and (25) as,

$$I(t) = I_{23} + \Delta I z(t) + \xi(t), \quad (26)$$

we see that $z(t)$ gives the two-qubit signal. In addition, for linear coupling $z(t)$ is equal to the average z -component of the total spin.

The unitary part has one contribution proportional to the Rabi frequency Ω , one proportional to the energy bias ε , and one proportional to the interqubit coupling U/\hbar :

$$\frac{d\rho_{ij}^B}{dt} \Big|_{H-evol} = \frac{d\rho_{ij}^B}{dt} \Big|_{\Omega} + \frac{d\rho_{ij}^B}{dt} \Big|_{\varepsilon} + \frac{d\rho_{ij}^B}{dt} \Big|_U \quad (27)$$

where

$$\frac{d\rho_{ij}^B}{dt} \Big|_{\Omega} = \Omega \begin{bmatrix} 0 & 0 & i\rho_{14}^B & i\rho_{13}^B \\ \cdot & 0 & i\rho_{24}^B & i\rho_{23}^B \\ \cdot & \cdot & -2\text{Im} \rho_{34}^B & i(\rho_{33}^B - \rho_{44}^B) \\ \cdot & \cdot & \cdot & 2\text{Im} \rho_{34}^B \end{bmatrix}, \quad (28)$$

$$\frac{d\rho_{ij}^B}{dt} \Big|_{\varepsilon} = \frac{\varepsilon}{\hbar} \begin{bmatrix} 0 & i\rho_{14}^B & 0 & i\rho_{12}^B \\ \cdot & -2\text{Im} \rho_{24}^B & -i\rho_{43}^B & i(\rho_{22}^B - \rho_{44}^B) \\ \cdot & \cdot & 0 & i\rho_{32}^B \\ \cdot & \cdot & \cdot & 2\text{Im} \rho_{24}^B \end{bmatrix}, \quad (29)$$

and

$$\frac{d\rho_{ij}^B}{dt} \Big|_U = 2\frac{U}{\hbar} \begin{bmatrix} 0 & i\rho_{12}^B & 0 & i\rho_{14}^B \\ \cdot & 0 & -i\rho_{23}^B & 0 \\ \cdot & \cdot & 0 & i\rho_{34}^B \\ \cdot & \cdot & \cdot & 0 \end{bmatrix}. \quad (30)$$

The state (10) which we have denoted $|1\rangle^B$ has spin-0, while the other three Bell states (11) - (13) comprise the spin-1 subspace. By inspecting Eqs. (23) and (24), one sees that measurement does not mix the spin-0 and spin-1 subspaces. Indeed, when the system is in the spin-0 subspace, $\rho_{11}^B = 1$, then $d\rho_{11}^B/dt$ vanishes (since $z = 0$). It also vanishes when the system is in the spin-1 subspace ($\rho_{11}^B = 0$). Since $\text{Tr}\rho^B = 1$, it follows that if the system is initially in the spin-1 subspace it will remain there. In the purely quadratic measurement case ($\delta = -2$) we have from (25) $z = -(\rho_{22}^B + \rho_{44}^B)$, and calculation shows that the spin-0 state $|1\rangle^B$, the state $|2\rangle^B$, and the “+” subspace, $\{|3\rangle^B, |4\rangle^B\}$, similarly do not mix. For unbiased qubits, $\varepsilon = 0$, Hamiltonian evolution via Eqs. (28) and (30) also neither mixes the spin-0 and spin-1 subspaces nor the three subspaces of the purely quadratic regime. Gradual collapse to one of these subspaces occurs during the qubit evolution as numerical simulation shows. In the linear and non-linear cases there are two collapse scenarios: collapse to the spin-0 or to the spin-1 subspace, so that the operator $(\vec{\sigma}^{(1)} + \vec{\sigma}^{(2)})^2$ is being effectively measured. In the purely quadratic case, there are three collapse scenarios; we can say that we are effectively measuring the operator $\sigma_y^{(1)}\sigma_y^{(2)} + \sigma_z^{(1)}\sigma_z^{(2)}$, whose eigenspaces are $|1\rangle^B$, $|2\rangle^B$, and the “+” subspace $\{|3\rangle^B, |4\rangle^B\}$ with eigenvalues -1 , 1 and 0 respectively. One can confirm using (22) that the measurement subspaces associated with these collapse scenarios are attractive. In other words, small deviations from a collapsed state tend toward zero under the evolution (22). Similar attraction was obtained previously in an analysis of a sequence of strong measurements.³⁴

We characterize below the collapse scenarios by calculating the probability of collapse, typical collapse time, and power spectrum of the detector current.

C. Collapse scenarios when $\varepsilon = 0$ and $U = 0$

1. Linear and non-linear detection

Examination of ensemble averaged equations (master equations) provides insight into the collapse scenarios. These equations can be obtained from (22) by simply eliminating the noise term (24). For both linear and non-linear detection, the master equations have the following stationary solution

$$\begin{aligned} \rho_{ij,st}^B &= 0, & \text{for } i \neq j \\ \rho_{11,st}^B &= \rho_{11}^B(0), \\ \rho_{22,st}^B &= \rho_{33,st}^B = \rho_{44,st}^B = \frac{1}{3}[1 - \rho_{11}^B(0)]. \end{aligned} \quad (31)$$

The solution $\langle \rho_{11}^B(t) \rangle$ of the ensemble averaged equations is a constant in time, $\langle \rho_{11}^B(t) \rangle = \rho_{11}^B(0)$. Taking into account that after some measurement time⁵² $t \gg \tau_{meas}$ all members of the ensemble eventually collapse to $\rho_{11}^B(t) = 1$ or $\rho_{11}^B(t) = 0$ it must be that the

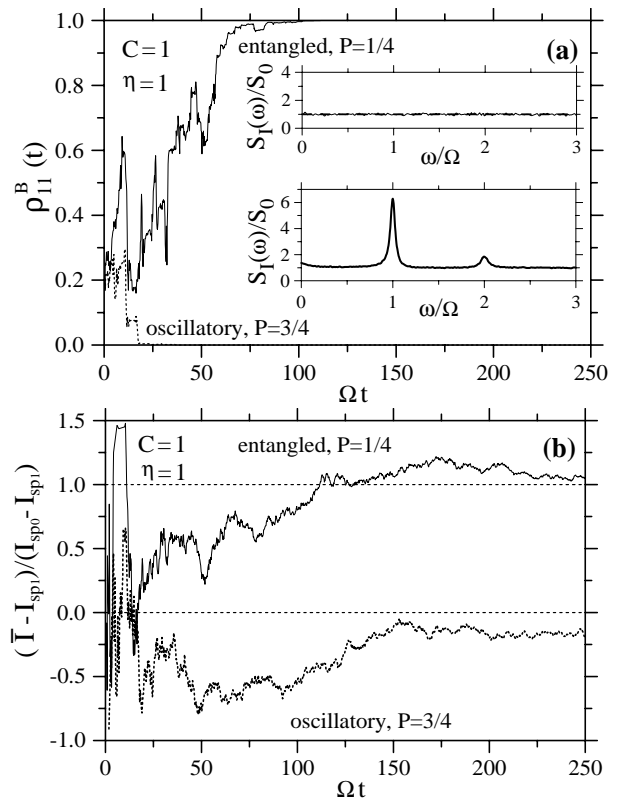


FIG. 3: Two numerical realizations of two-qubit evolution starting from the fully mixed state for a *non-linear measurement*, $\delta = -1$, by an ideal ($\eta = 1$) detector. (a) Evolution of ρ_{11}^B . The upper (solid) line illustrates the scenario of collapse into the entangled Bell state $|1\rangle^B$, while the lower (dotted) line shows a collapse into the orthogonal subspace. The two insets show the corresponding spectral densities $S_I(\omega)$ of the detector current. (b) The detector current \bar{I} averaged over the whole time starting from $t = 0$ is shown for the same collapse scenarios as in (a). Dashed horizontal lines correspond to the normalized averaged currents I_{sp0} , I_{sp1} .

fraction of members that collapse to $\rho_{11}^B(t) = 1$ is equal to $\langle \rho_{11}^B(t) \rangle$. Thus, one expects that the probability of collapse to the spin-0 subspace is $\rho_{11}^B(0)$, while the probability of collapse to the spin-1 subspace is $1 - \rho_{11}^B(0)$.

Extensive Monte Carlo simulations of (22) were performed for weak coupling (\mathcal{C} between 1/4 and 1). As illustrated in Fig. 3, they show that any initial state either collapses eventually into the spin-0 state or collapses to the orthogonal, spin-1 subspace within which it performs oscillations. Within a level of accuracy consistent with the number of trials, the probability of evolving into the Bell state $|1\rangle^B$ coincides with the initial value $\rho_{11}^B(0)$. In particular, starting from a completely mixed state the probability is $\rho_{11}^B(0) = 1/4$.

We can monitor the process of collapse of $\rho_{ij}(t)$ through the Bayesian equation (6) for a given measurement result $I(t)$. Collapse is also revealed in the appearance of different power spectra for $I(t)$ depending upon the final state (insets in Fig. 3(a)). In the case of col-

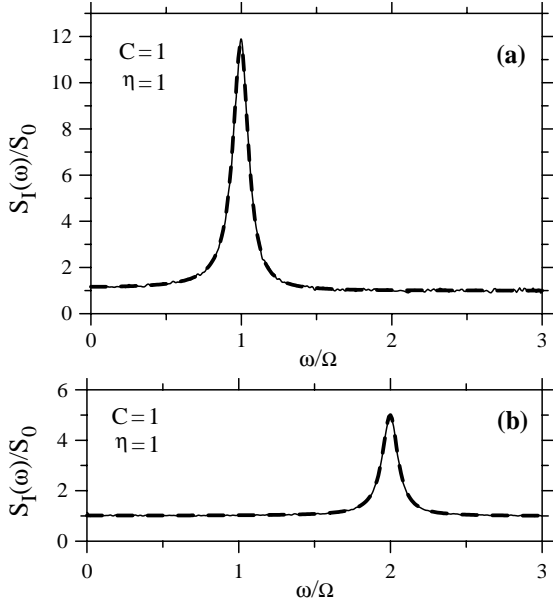


FIG. 4: The two-qubit power spectrum in the oscillating scenario in the linear (a) and purely quadratic (b) detection regimes. Analytical calculation (dashed line), given by Eqs. (47),(49) practically coincides with numerics.

lapse to the entangled state $|1\rangle^B$, the spectrum is flat and coincides with the shot noise spectral density S_0 . In the case of collapse to the spin-1 subspace, the qubit performs oscillations within the subspace. In the linear case the oscillations lead to a single peak in the power spectrum (Fig. 4(a)) at the Rabi frequency Ω with peak height $(32/3)S_0$ and width $\Gamma = (\Delta I)^2/4S_0$ that is confirmed analytically below. In the general non-linear case, one sees peaks in the power spectrum at the Rabi frequency Ω and also at zero and double the Rabi frequency (Fig. 3(a), lower inset).

The average detector current using (7) is $\langle I(t) \rangle = \sum_k I_k \langle \rho_{kk}(t) \rangle_t$. After collapse, the time average $\langle \rho_{kk}(t) \rangle_t$ can be calculated using the stationary ensemble averaged solution (31) – the initial transient period of the order of the measurement time can be neglected. In the spin-0 scenario one finds $\langle \rho_{22}(t) \rangle_t = \langle \rho_{33}(t) \rangle_t = 1/2$, implying $\langle I(t) \rangle = I_{sp0} = (I_2 + I_3)/2 = I_{23}$. In the spin-1 scenario $\langle \rho_{11}(t) \rangle_t = \langle \rho_{44}(t) \rangle_t = 1/3$ and $\langle \rho_{22}(t) \rangle_t = \langle \rho_{33}(t) \rangle_t = 1/6$, so that $\langle I(t) \rangle = I_{sp1} = (I_1 + I_{23} + I_4)/3$. In the linear case (Fig. 2), the average current in the detector is the same in both scenarios ($\langle I(t) \rangle = I_{sp0} = I_{sp1} = I_{23}$) since $I_{23} = (I_1 + I_4)/2$. Therefore the spin-0 and spin-1 subspaces are indistinguishable by average currents and we have to measure the power spectrum in order to distinguish them. In Appendix B we have evaluated the typical time needed to accumulate the spectral peak; it is on the order of $1/\Gamma\eta^2$.

In the non-linear case, the final state can be identified by the average current in the detector: $I_{sp0} = I_{23}$ in the spin-0 scenario and $I_{sp1} = (I_1 + I_{23} + I_4)/3$ in the oscillating spin-1 case (Fig. 3(b)). Thus one expects the current

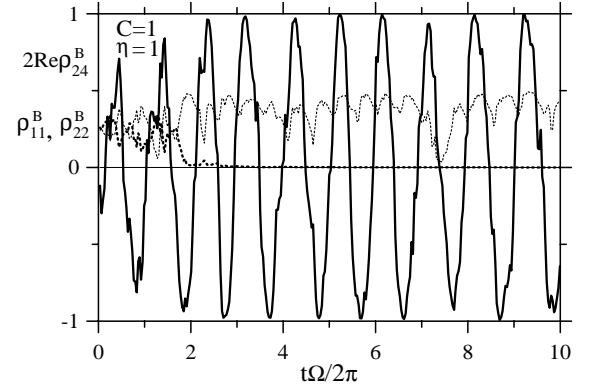


FIG. 5: Linear weak ideal measurement. State purification in case of oscillating spin-1 collapse scenario ($\rho_{11}^B \rightarrow 0$, thick dashed line) starting from a fully mixed state. The qubits signal $z = 2\text{Re}\rho_{24}^B$, Eq. (25) establishes quantum oscillations at Rabi frequency (thick solid line) with slowly fluctuating amplitude and phase. Also shown are fluctuations of ρ_{22}^B (thin dotted line).

signal averaged over sufficiently long times $\Delta t \gtrsim 1/\Omega$, $\bar{I} = (1/\Delta t) \int_0^{\Delta t} I(t') dt'$, to be Gaussian distributed with average either I_{23} or $(I_1 + I_{23} + I_4)/3$ and with variance $S_0/2\Delta t$. We have confirmed this conjecture by numerical simulations of the detector current. As a result, the typical time necessary to distinguish between the two scenarios with a signal-to-noise ratio of 1 is on the order²⁶ of $\tau_{meas} = 2S_0/(I_{sp0} - I_{sp1})^2 = 18S_0/(2I_{23} - I_1 - I_4)^2$. This estimate is self-consistent since we are working in the weak coupling regime ($\Gamma \ll \Omega$), so that the measurement time $\tau_{meas} \gg 1/\Omega$. Hence, for $\Delta t \sim \tau_{meas}$, the current \bar{I} in the oscillating scenario is effectively averaged to the value I_{sp1} over many periods of oscillation.

Both in linear and non-linear cases when collapse to $|1\rangle^B$ occurs, purification of the state is clearly inevitable even for a non-ideal detector with $\eta < 1$. Simulation (see Fig. 5) shows that for an ideal detector, the qubit state purifies also in the case of collapse to the spin-1 subspace. (Such purification during oscillation in the weak measurement regime is similar to the purification in the one-qubit case;²⁶ for analogous purification in the case of measurement of an oscillator, see Ref. 41). After initial relaxation, the surviving nondiagonal matrix elements in the Bell basis are found numerically to satisfy

$$(\text{Re}\rho_{24}^B)^2 = \rho_{22}^B \rho_{44}^B, \quad (\text{Im}\rho_{23}^B)^2 = \rho_{22}^B \rho_{33}^B, \quad (32)$$

$$(\text{Im}\rho_{34}^B)^2 = \rho_{33}^B \rho_{44}^B \quad (32)$$

$$\text{Im}\rho_{24}^B = \text{Re}\rho_{23}^B = \text{Re}\rho_{34}^B = 0 \quad (33)$$

which imply that the pure-state condition $\rho^2 = \rho$ is satisfied by the matrix ρ .

In the weak coupling case $\mathcal{C} \lesssim 1$ for a linear ideal detector ($\eta = 1$) it is possible to characterize further the evolution of the density matrix. Since purification of the state leads to Eqs. (32) and (33), of the 8 real degrees of freedom in the density matrix of the collapsed system,

only 2 remain independent. The system oscillates with slowly fluctuating amplitude and phase (see Fig. 5). Taking into account the free Hamiltonian evolution, Eq. (28), we can write

$$z = 2\text{Re}\rho_{24}^B = A(t) \cos(\Omega t + \varphi(t)), \quad (34)$$

$$y \equiv 2\text{Im}\rho_{23}^B = A(t) \sin(\Omega t + \varphi(t)), \quad (35)$$

$$z_1 \equiv \rho_{33}^B - \rho_{44}^B = -B(t) \cos(2\Omega t + 2\varphi(t)), \quad (36)$$

$$y_1 \equiv 2\text{Im}\rho_{34}^B = -B(t) \sin(2\Omega t + 2\varphi(t)). \quad (37)$$

Here, $A(t) = 2\sqrt{\rho_{22}^B(1 - \rho_{22}^B)}$ and $B(t) = 1 - \rho_{22}^B$, so it is natural to regard $\rho_{22}^B(t)$ and $\varphi(t)$ as the two independent variables. The quantities $A(t)$, $B(t)$, and $\varphi(t)$ are constants in the absence of measurement while in the presence of measurement they slowly fluctuate in time. (The stationary distribution of ρ_{22}^B is calculated in Appendix A.) Eqs. (34)-(37) complete the description of the collapse subspaces in the case of weak linear ideal measurements.

2. Purely quadratic detection

In the case of purely quadratic measurement ($I_1 = I_4 \equiv I_{14}$, $\delta = -2$), the stationary solution of the master equation is

$$\begin{aligned} \rho_{ij,st}^B &= 0, & \text{for } i \neq j \\ \rho_{11,st}^B &= \rho_{11}^B(0), & \rho_{22,st}^B = \rho_{22}^B(0) \\ \rho_{33,st}^B &= \rho_{44,st}^B = \frac{1}{2}[1 - \rho_{11}^B(0) - \rho_{22}^B(0)]. \end{aligned} \quad (38)$$

This suggests that with probability $\rho_{11}^B(0)$ the system collapses under measurement to $|1\rangle^B$, with probability $\rho_{22}^B(0)$ the system collapses to $|2\rangle^B$, and with probability $1 - \rho_{11}^B(0) - \rho_{22}^B(0)$ the system collapses to the remaining subspace.

Numerical simulations verify these three collapse scenarios. The average currents are I_{23} , I_{14} , and $(I_{23} + I_{14})/2$ for the three scenarios so that the current spacing is $\Delta I/2$. In the case of collapse to the two-dimensional $\{|3\rangle^B, |4\rangle^B\}$ subspace, the two-qubit system performs quantum oscillations as seen in Eq. (15). At times larger than the oscillation period (that are relevant in the weak measurement regime) we can estimate a typical time necessary to distinguish between the three scenarios that is on the order of $\tau_{meas} \approx 8S_0/(\Delta I)^2$.

We checked numerically that the probabilities of the three collapse scenarios are given by the initial values $\rho_{11}^B(0)$, $\rho_{22}^B(0)$, and $1 - \rho_{11}^B(0) - \rho_{22}^B(0)$ respectively. In the case of collapse to the two-dimensional subspace, the qubits oscillate, producing one peak in the power spectrum at double the Rabi frequency (Fig. 4(b)), with peak height $4S_0$ and width $\Gamma = (\Delta I)^2/4S_0$.

It is interesting to note the difference between the weak measurement results presented here and the hypothetical (experimentally difficult) strong measurement case.

A strong, purely quadratic measurement was suggested in Ref. 38 as a means of measuring the relative state of two qubits for use in error correction procedures. In the strong measurement case the qubit Hamiltonian dynamics is much slower than the measurement dynamics – the measurement occurs within a time much shorter than the qubit oscillation period $\tau_{meas} \sim S_0/(\Delta I)^2 \ll 2\pi/\Omega$. As a result, the two-qubit system collapses to subspaces with average current I_{14} or I_{23} , corresponding to “parallel” or “anti-parallel” qubits (Fig. 2), given in the Bell basis by $\{|2\rangle^B, |4\rangle^B\}$ and $\{|1\rangle^B, |3\rangle^B\}$. Therefore, effectively, the operator $\sigma_z^{(1)}\sigma_z^{(2)}$ is measured. In the weak measurement situation considered in this paper, the measurement time is much longer than the qubit oscillation period $\tau_{meas} \gg 2\pi/\Omega$. During the measurement, a well-defined averaged current $(I_{23} + I_{14})/2$ appears. Therefore, one can distinguish three subspaces leading to effective measurement of the operator $\sigma_y^{(1)}\sigma_y^{(2)} + \sigma_z^{(1)}\sigma_z^{(2)}$. Contrary to naive expectation, weak measurements taken for a long period of time are not equivalent to a strong measurement because of non-trivial interplay between the qubit Hamiltonian dynamics and dynamics due to the measurement process.

D. Correlator of measurement current and power spectrum when $\epsilon = 0$ and $U = 0$

In this subsection we derive the current correlation function and power spectrum of the detector signal for weak measurement of two identical qubits symmetrically coupled to the detector. It follows from (25) and (26) that after collapse to a one-dimensional subspace (to $|1\rangle^B$ in the linear and non-linear detector cases and to $|1\rangle^B$ or $|2\rangle^B$ in the purely quadratic case) the value of z is constant, the qubits do not oscillate, and the correlation function $K_I(\tau) = \langle I(t)I(t+\tau) \rangle - \langle I \rangle^2$ contains only the noise. The corresponding power spectrum is flat. Collapse to a higher-dimensional subspace (the three-dimensional spin-1 subspace in the linear detector case and the two-dimensional $\{|3\rangle^B, |4\rangle^B\}$ subspace in the purely quadratic case) leads to oscillations and a richer power spectrum that we derive below.

1. Linear detection

In the case of collapse to the spin-1 subspace in the linear case, we have $\langle I \rangle = I_{23}$ and from Eq. (25), $z = \rho_{11} - \rho_{44} = 2\text{Re}\rho_{24}^B$. Using expression (26), we have

$$K_I(\tau > 0) = (\Delta I)^2 K_z(\tau) + \Delta I K_{\xi z}(\tau). \quad (39)$$

First, we calculate the “back-action correlator” $K_{\xi z}(\tau) = \langle \xi(t)z(t+\tau) \rangle_t$ for $\tau > 0$. In an individual realization, the quantum back action on the qubit state ρ_{ij} is taken into account explicitly through the Bayesian equations (6). In particular, $\rho_{ij}(t+\tau)$ is correlated with

noise fluctuations of the current at some previous moment t (compare with Ref. 51). Indeed, a noise fluctuation $\xi(t)$ leads to a perturbation of the density matrix $\rho_{ij}(t)$ in the immediate vicinity of the time instant t , i.e., $\rho_{ij}(t+0) = \rho_{ij}(t) + d\rho_{ij}(t)$. The leading perturbation is given by Eq.(24)

$$dz(t) \simeq -2\frac{\Delta I}{S_0} [z^2(t) - (\rho_{22}^B(t) + \rho_{44}^B(t))] \xi(t) dt \quad (40)$$

$$dy(t) \simeq -2\frac{\Delta I}{S_0} [y(t)z(t) + y_1(t)/2] \xi(t) dt \quad (41)$$

where $y = 2\text{Im}\rho_{23}^B$ and $y_1 \equiv 2\text{Im}\rho_{34}^B$.

We proceed further by implicitly assuming that the long time average $\langle \dots \rangle_t$ is represented as three subsequent averages. First, averaging over different realizations of the stochastic process $\rho_{ij}(t')$ in the interval $t < t' < t + \tau$ is equivalent, assuming stationarity and ergodicity, to using the master equations for $z(t)$ and $y(t)$

$$\dot{z} = -\Omega y, \quad \dot{y} = \Omega z - \Gamma y. \quad (42)$$

The ensemble dephasing rate is $\Gamma = \eta^{-1}(\Delta I)^2/4S_0$. Note that the solution to the master equations is linear with respect to initial conditions. Explicitly, for $z(t)$ we have:

$$\begin{aligned} z(t) &= z(0) \exp(-\Gamma\tau/2) [\cos \tilde{\Omega}\tau + (\Gamma/2\tilde{\Omega}) \sin \tilde{\Omega}\tau] \\ &\quad - y(0) \exp(-\Gamma\tau/2) [\Omega/\tilde{\Omega}] \sin \tilde{\Omega}\tau \\ &\equiv z(0) G_z(\tau) + y(0) G_y(\tau), \end{aligned} \quad (43)$$

where $\tilde{\Omega} \equiv (\Omega^2 - \Gamma^2/4)^{1/2}$, and $G_z(\tau)$, $G_y(\tau)$ are the corresponding Green's functions. Therefore, the initial perturbation that appears due to $\xi(t)$, propagates to the later moment $t + \tau$ according to Eq. (43) with "initial" conditions $dz(t)$ and $dy(t)$: $\delta z(t + \tau) = dz(t) G_z(\tau) + dy(t) G_y(\tau)$. The second averaging is the standard averaging over noise (at instant t) according to $\langle \xi(t)\xi(t)dt \rangle = S_0/2$. The quantum correlation is expressed then as:

$$\begin{aligned} \langle \xi(t) z(t + \tau) \rangle &= \langle \xi(t) \delta z(t + \tau) \rangle \\ &= \Delta I [\langle \rho_{22}^B(t) + \rho_{44}^B(t) - z^2(t) \rangle G_z(\tau) \\ &\quad + \langle y(t) z(t) + y_1(t)/2 \rangle G_y(\tau)]. \end{aligned} \quad (44)$$

A third averaging over the "initial" condition $\rho_{ij}^B(t)$ remains to be done.

The calculation for the correlation $K_z(\tau) = \langle z(t)z(t + \tau) \rangle_t$ also proceeds in stages, first averaging over different realizations for $\rho_{ij}(t')$ in the interval $t < t' < t + \tau$. Then

$$\langle z(t) z(t + \tau) \rangle = \langle z^2(t) \rangle G_z(\tau) - \langle y(t) z(t) \rangle G_y(\tau). \quad (45)$$

In (39) the unknown averages $\langle z^2(t) \rangle$ and $\langle y(t) z(t) \rangle$ cancel out, and $\langle y_1 \rangle = 0$, so we obtain

$$K_I(\tau) = (\Delta I)^2 \langle \rho_{22}^B + \rho_{44}^B \rangle G_z(\tau) = (\Delta I)^2 \frac{2}{3} G_z(\tau), \quad (46)$$

where we have used stationary values from (31). This is valid for arbitrary coupling \mathcal{C} and detector ideality η .

The corresponding current spectral density $S_I(\omega) = 2 \int_{-\infty}^{\infty} K_I(\tau) \exp(i\omega\tau) d\tau$ is readily computed by Fourier transform³⁴ to be

$$S_I(\omega) = S_0 + \frac{8}{3} \frac{\Omega^2(\Delta I)^2\Gamma}{(\omega^2 - \Omega^2)^2 + \Gamma^2\omega^2}. \quad (47)$$

In the case of weak coupling, $\Gamma \ll \Omega$, the spectral peak is at Ω ; it has the same width as in the one-qubit case³⁰ and peak height $(32/3)\eta S_0$, which we have confirmed in numerical simulations (Fig. 4(a)). It is important to emphasize that in an ensemble averaged approach starting from a totally mixed state this power spectrum would be weighted by 3/4, the probability of collapse into the spin-1 subspace. The averaged peak height would therefore be $8\eta S_0$. To derive the higher value of $(32/3)\eta S_0$ one must analyze a two-qubit system already collapsed into the spin-1 subspace.

2. Purely quadratic detection

For purely quadratic detection, the system can collapse to $|1\rangle^B$ or to $|2\rangle^B$, or it can collapse to the subspace $\{|3\rangle^B, |4\rangle^B\}$ and perform oscillations. In this last scenario, $\rho_{11}^B(t) = \rho_{22}^B(t) = 0$ and $\langle I \rangle = I_{23} - \Delta I/2$. To study the oscillating signal, it is convenient to rewrite Eq. (26) in the form $I(t) = \langle I \rangle + (\Delta I/2) z_1(t) + \xi(t)$ where $z_1(t) \equiv \rho_{33}^B(t) - \rho_{44}^B(t)$. The Itô equations for the relevant density matrix components $z_1(t)$ and $y_1(t)$ again decouple from all other components appearing in Eq. (23)–(30). The corresponding master equations read

$$\dot{z}_1 = -2\Omega y_1, \quad \dot{y}_1 = 2\Omega z_1 - \Gamma y_1. \quad (48)$$

Significantly, motion in this two dimensional Hilbert space is precisely analogous to one-qubit motion³⁰, but with the oscillation frequency 2Ω rather than Ω . This is natural because quadratic measurement is sensitive only to the relative state of the two qubits distinguishing only between states with "parallel" and "anti-parallel" spins.

Applying the same steps as in Eqs. (40)–(45), we obtain the power spectrum

$$S_I(\omega) = S_0 + \frac{4\Omega^2(\Delta I)^2\Gamma}{(\omega^2 - 4\Omega^2)^2 + \Gamma^2\omega^2}, \quad (49)$$

that exhibits a peak at 2Ω with height $4\eta S_0$ and width $\Gamma = (\Delta I)^2/4\eta S_0$ just as in the linear case.^{30,48,53,54} In an ensemble averaged approach, starting from totally mixed state the peak height of (49) would be weighted by 1/2, the probability that a totally mixed system will collapse into the subspace $\{|3\rangle^B, |4\rangle^B\}$. Thus the peak height would be $2\eta S_0$; it is necessary to analyze a two-qubit system known to have collapsed to the oscillating subspace to predict the larger height of $4\eta S_0$.

E. Influence of bias ϵ and two-qubit coupling U

We now discuss the influence of non-zero energy bias $\epsilon_a = \epsilon_b = \epsilon$ and two-qubit coupling U for identical qubits. Numerical simulations and analytical calculations both show that the system still collapses and purifies. However, differences arise in the collapse scenarios.

In the case of a linear detector, the system will still collapse to the spin-0 subspace $|1\rangle^B$ or to the spin-1 subspace $\{|2\rangle^B, |3\rangle^B, |4\rangle^B\}$. In fact, the corresponding stationary solution, Eq. (31), remain unchanged. This is because the additional evolution due to ϵ - and U -terms, Eqs. (29) and (30), does not mix the two subspaces.

The characteristics of the spin-0 collapse scenario are not affected by the parameters ϵ and U . In particular, the resulting power spectrum is still flat with $S_I(\omega)$ equal to the detector shot noise S_0 .

In the oscillating, spin-1 scenario the additional dynamics do influence the form of the spectral density $S_I(\omega)$. For $U = 0$ the relevant master equations are

$$\begin{aligned} \dot{z} &= -\Omega y, & \dot{y} &= \Omega z - \Gamma y - (\epsilon/\hbar)x, \\ \dot{x} &= -\Gamma x + (\epsilon/\hbar)y \end{aligned} \quad (50)$$

with $x \equiv 2\text{Re}\rho_{34}^B$ and y, z as in Eq. (42). This is exactly the same system of equations as in the one-qubit case with a non-zero bias. Thus, the corresponding spectral density in the two-qubit case is related to the one-qubit spectral density peak, $\tilde{S}_I^{1qb}(\omega, \Omega, \Gamma, \epsilon) \equiv S_I^{1qb} - S_0$, considered in Refs. 30,48

$$S_I^{2qb-linear}(\omega, \Omega, \Gamma, \epsilon) = S_0 + \frac{8}{3} \tilde{S}_I^{1qb}(\omega, \Omega, \Gamma, \epsilon). \quad (51)$$

As in the one-qubit case, finite ϵ leads to a decrease of the spectral peak around the Rabi frequency Ω and to the emergence of an extra peak around zero frequency. Note, that the 8/3 enhancement factor is just as in the zero bias case, Eq. (47). Numerical simulations of Eqs. (23)–(29) confirm this result.

For $\epsilon = 0$ and $U \neq 0$, the form of the spectral peak(s) in the oscillating scenario can be calculated either by numerical simulations using Bayesian Eqs. (23)–(30) or through an ensemble average method developed in Refs. 35,36. Increasing U from zero first suppresses and then splits the spectral peak at the Rabi frequency Ω .

In the case of purely quadratic detection, qubit biasing so that $\epsilon \neq 0$ while $U = 0$ will lead to mixing between the $|2\rangle^B$ and $\{|3\rangle^B, |4\rangle^B\}$ subspaces as seen from Eq. (29). For small bias ϵ this will take the form of rare switching events whose rate and influence on the spectrum will be discussed in the next section.

If $U \neq 0$ while $\epsilon = 0$, one notices that the density matrix components $z_1(t) \equiv \rho_{33}^B(t) - \rho_{44}^B(t)$, $y_1(t) \equiv 2\text{Im}\rho_{34}^B$, and $x \equiv 2\text{Re}\rho_{34}^B$ obey equations analogous to (50) in which Ω is replaced by 2Ω , z by z_1 , y by y_1 , and ϵ by $2U$. Thus, the form of the spectrum is described with the same functional form, as in Eq. (51)

$$S_I^{2qb-quadr}(\omega) = S_0 + \tilde{S}_I^{1qb}(\omega, 2\Omega, \Gamma, 2U). \quad (52)$$

The result is a decrease of the spectral peak at 2Ω seen in Eq. (49) and the appearance of a peak at zero frequency. This finding is confirmed by numerical simulations.³⁵

IV. QUANTUM ZENO-LIKE STABILIZATION

The quantum Zeno effect is usually understood to arise in the case of projective measurements taken more and more frequently. In our case of continuous measurement the detector is always coupled to the system, so the approach to the quantum Zeno regime corresponds instead to the limit of stronger and stronger coupling. Since it is impractical to realize strong coupling detectors in many systems (the dimensionless coupling to each qubit, $\mathcal{C} \sim \Gamma/\Omega$, is typically small), one might not expect quantum Zeno physics to arise. However, in our system of two identical qubits, a small perturbative asymmetry between the qubits, such as when $\Delta\Omega = \Omega_a - \Omega_b \neq 0$, can generate slow transitions between states that were uncoupled. The effective coupling for this dynamical process, $\mathcal{C}_{eff} \sim \Gamma/\Delta\Omega$, can be very large, leading to a Zeno effect.

From this perspective, the symmetric-qubit situation, $\Delta\Omega = 0$, constitutes the Zeno limit of infinitely large coupling \mathcal{C}_{eff} ; the transition becomes completely inactive, and the quantum state becomes “frozen”. The asymmetric situation with non-zero $\Delta\Omega$ implies finite effective coupling \mathcal{C}_{eff} . The non-zero $\Delta\Omega$ makes the quantum state to “decay” from one subspace to another. But, since the coupling is large, the decay of the quantum state looks like an abrupt *switching event*, with duration on the order of the measurement time $\tau_{meas} \sim 1/\Gamma$, rather than gradual evolution of frequency $\Delta\Omega$. The switching event can be identified experimentally by measuring the power spectrum, for instance. From an ensemble averaged point of view, at long times the decay becomes exponential with a rate that is much smaller than Γ .

Numerical simulations using Bayesian equations (6) confirm that the two-qubit density matrix ρ experiences rare, abrupt switching between different subspaces when the qubits have a slight asymmetry like a non-zero $\Delta\Omega$. These switchings are apparent in Figs. 6 and 7. Switching also happens for identical qubits when there is small difference of couplings $\mathcal{C}_a, \mathcal{C}_b$ to the detector (due to different values for ΔI_a and ΔI_b) or different coupling to an environment.

For linear detection the switching occurs between the spin-0 and spin-1 subspaces while for quadratic measurement we will have three-terminal switching among the three collapse subspaces described above. The switching events can be directly observed through measurement of the *intermediate time scale* power spectrum and/or average detector currents. (Such intermediate time observables are meaningful if the measurement time needed to accumulate the spectrum is much smaller than the “lifetime” of the subspaces.) If measurement is performed for a sufficiently long time, it will lead to averaging of the spectrum and may also lead to the appearance of an

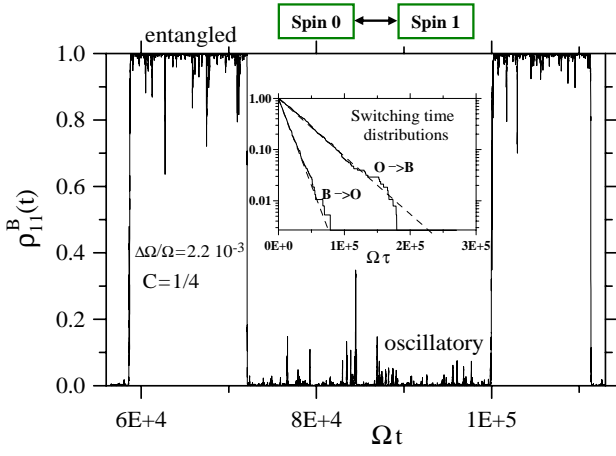


FIG. 6: *Linear detection.* Switching between spin-0 and spin-1 subspaces as seen in the time evolution of $\rho_{11}^B(t)$, in case of different Rabi frequencies. The parameters are: $C = 1/4$, and $\Delta\Omega/\Omega \simeq 2.2 \times 10^{-3}$. The inset shows numerical histograms (in logarithmic scale) of switching time distributions in agreement with the asymptotic switching rates Eqs. (58), (63).

additional telegraph noise peak at zero frequency analogous to the regime of strong coupling in the one-qubit case.^{30,31}

A. Perturbation to the qubits

To find the switching rates analytically, we have used the master equation, which reads of Eqs. (23)–(29)

$$\frac{d\rho_{ij}^B}{dt} = \left. \frac{d\rho_{ij}^B}{dt} \right|_{meas} + \left. \frac{d\rho_{ij}^B}{dt} \right|_{\Omega} + \left. \frac{d\rho_{ij}^B}{dt} \right|_{\varepsilon} + \left. \frac{d\rho_{ij}^B}{dt} \right|_U$$

with the noise term (24) omitted from $d\rho_{ij}^B/dt|_{meas}$. It now acquires additional terms. When the frequencies of the two qubits are slightly different while coupling to the detector is symmetric, $I_2 = I_3$, we have in addition to Eq. (28)

$$\left. \frac{d\rho_{ij}^B}{dt} \right|_{H-evol, H_a \neq H_b} = \frac{\Delta\Omega}{2} \times \begin{pmatrix} -2\text{Im}\rho_{12}^B & i(\rho_{11}^B - \rho_{22}^B) & -i\rho_{23}^B & -i\rho_{24}^B \\ \cdot & 2\text{Im}\rho_{12}^B & -i\rho_{13}^B & -i\rho_{14}^B \\ \cdot & \cdot & 0 & 0 \\ \cdot & \cdot & \cdot & 0 \end{pmatrix} \quad (53)$$

and in addition to Eq. (29)

$$\left. \frac{d\rho_{ij}^B}{dt} \right|_{H-evol, \varepsilon_a \neq \varepsilon_b} = -\frac{(\Delta\varepsilon/\hbar)}{2} \times \begin{pmatrix} 2\text{Im}\rho_{13}^B & i\rho_{32}^B & -i(\rho_{11}^B - \rho_{33}^B) & i\rho_{34}^B \\ \cdot & 0 & -i\rho_{21}^B & -i(\rho_{22}^B - \rho_{44}^B) \\ \cdot & \cdot & -2\text{Im}\rho_{13}^B & i\rho_{14}^B \\ \cdot & \cdot & \cdot & 0 \end{pmatrix}. \quad (54)$$

1. Linear detection

For linear detection ($\delta = 0$), assuming weak coupling $\Delta\Omega \ll \Gamma \ll \Omega$ and unbiased, non-interacting qubits $\varepsilon_a = \varepsilon_b = U = 0$, a system of equations for the quantities $\rho_{11}^B - \rho_{22}^B$, $2\text{Im}\rho_{12}^B$, $\rho_{22}^B - \rho_{44}^B$, $\rho_{33}^B - \rho_{44}^B$, and $2\text{Im}\rho_{34}^B$ can be extracted from Eqs. (23)–(29) and (53). To change them into a system of master equations for ensemble averages, we simply set the noise term to zero $\xi = 0$ in (23). Starting from the entangled initial condition $\rho_{11}^B(0) = 1$ we find $\rho_{11}^B(t) = 1 - \frac{(\Delta\Omega)}{2} \int_0^t dt' 2\text{Im}\rho_{12}^B(t')$. Formal integration of the equation for $2\text{Im}\rho_{12}^B$ (see Eqs. (23), (53)) leads to the exact relation

$$\rho_{11}^B(t) = 1 - \frac{(\Delta\Omega)^2}{2} \int_0^t dt' e^{-\Gamma t'} \times \int_0^{t'} dt'' e^{\Gamma t''} (\rho_{11}^B(t'') - \rho_{22}^B(t'')). \quad (55)$$

Solving our system of master equations to zeroth order in $\Delta\Omega$ and substituting into (55), we obtain an approximate solution for the “survival probability,” $\rho_{11}^B(t)$:

$$\rho_{11}^B(t) = 1 + \frac{(\Delta\Omega)^2}{2\Gamma^2} - \frac{(\Delta\Omega)^2}{2\Gamma} t - \frac{(\Delta\Omega)^2}{2\Gamma^2} \exp(-\Gamma t). \quad (56)$$

For times $t \ll 1/\Gamma$, one can expand the exponential and find that there is no linear term in the t -expansion of (56). This fact makes quantum Zeno effect physics possible.^{4,5,6} The first few terms in the small t -expansion of (56) actually coincide with the exact small t -expansion of $\rho_{11}^B(t)$ derived directly from the master equations by differentiation, using the initial conditions

$$\rho_{11}^B(t) = 1 - \frac{(\Delta\Omega)^2}{4} t^2 + \frac{(\Delta\Omega)^2 \Gamma}{12} t^3 - \dots \quad (57)$$

The t^2 -coefficient turns out to be $-(\Delta\Omega)^2/4 = -\text{Tr}[\hat{\rho}^2 \mathcal{H}_{QB}^2] + \text{Tr}[\hat{\rho} \mathcal{H}_{QB} \hat{\rho} \mathcal{H}_{QB}]$, i.e. it is determined by coherent (Hamiltonian) evolution alone consistent with the discussions in Refs. 4,5,6. One might speculate that the system has some memory at the time scale $t \ll 1/\Gamma$, “forgetting” its history once $t \gtrsim \Gamma^{-1}$ when the exponential term in Eq. (56) drops out. At still longer times, the “decay” from the Bell state to the oscillating subspace eventually becomes exponential with rate

$$\Gamma_{B \rightarrow O}^{H_a \neq H_b} = \frac{(\Delta\Omega)^2}{2\Gamma} \quad (58)$$

as demonstrated by switching time distributions shown at the inset of Fig. 6. Note, that the switching rate in (58) is similar to the one-qubit case³⁰ with the replacement $\Omega \rightarrow \Delta\Omega$.

An analogous derivation for the case of different qubit biases $\varepsilon_a \neq \varepsilon_b$ can be performed. We set $\varepsilon = (\varepsilon_a + \varepsilon_b)/2 = 0$ since effects of having $\varepsilon \neq 0$ (while $\varepsilon_a = \varepsilon_b$) have been considered above, in Sec. III E. We stipulate that

$|\Delta\varepsilon|/\hbar \ll \Omega$ but permit $|\Delta\varepsilon|/\hbar$ and Γ to be of the same order. From (28), (54) we find

$$\dot{\rho}_{11}^B(t) = -(\Delta\varepsilon/\hbar) \text{Im}\rho_{13}^B = \dot{x}_{13}(t)/2, \quad (59)$$

where $x_{13}(t) \equiv \rho_{11}^B(t) - \rho_{33}^B(t)$. The second equality in (59) was obtained by solving a system of nine equations extracted from Eqs. (23), (28), and (54), using the initial condition $\rho_{11}^B(0) = 1$. These nine equations quickly reduce to a system of three equations for $2 \text{Im}\rho_{13}^B$, $2 \text{Re}\rho_{14}^B$, and $x_{13} \equiv \rho_{11}^B - \rho_{33}^B$, which can be solved perturbatively in $\Delta\varepsilon/\hbar$. Integrating (59), we obtain $\rho_{11}^B(t) = (1+x_{13}(t))/2$. An approximate solution for $\rho_{11}^B(t)$ is

$$\rho_{11}^B(t) = 1 - b_\varepsilon \frac{\Gamma}{2} t + \frac{b_\varepsilon c_\varepsilon}{2} - \frac{b_\varepsilon}{2} \exp(-\Gamma t/2) \times \left[c_\varepsilon \cos \tilde{\Omega} t - \frac{\Gamma}{2\tilde{\Omega}} [2 - c_\varepsilon] \sin \tilde{\Omega} t \right], \quad (60)$$

where $b_\varepsilon \equiv (\Delta\varepsilon/\hbar)^2 / [\Omega^2 + (\Delta\varepsilon/\hbar)^2]$, $c_\varepsilon \equiv \Gamma^2 / [\Omega^2 + (\Delta\varepsilon/\hbar)^2] - 1$, and $\tilde{\Omega} \equiv \sqrt{\Omega^2 + (\Delta\varepsilon/\hbar)^2 - \Gamma^2/4}$. As in (57), there is no linear term; the evolution is quadratic in t at small times permitting quantum Zeno effect physics.⁶ The decay is exponential on a coarse time scale $t \gtrsim 2\Gamma^{-1}$ with switching rate

$$\Gamma_{B \rightarrow O}^{\varepsilon_a \neq \varepsilon_b} = \frac{(\Delta\varepsilon/\hbar)^2 \Gamma}{2\Omega^2}. \quad (61)$$

Numerical solution of the master equations for the density matrix confirms these results.

We have computed the rate of switching from the spin-0 Bell state $|1\rangle^B$ to the spin-1 subspace. To compute the rate of reverse switching, we notice that the stationary solution of the master equations (Eqs. (23)–(30), (53), and (54) with the noise ξ set to zero) has the form

$$\rho_{ij, st}^B = \rho_{ij, st} = \delta_{ij}/4. \quad (62)$$

This form is completely mixed because (53) and (54) cause transitions between the spin-0 and spin-1 subspaces. One infers that the system should spend on average 1/4 of the time in the state $|1\rangle^B$, suggesting the stationary state condition $(1/4)\Gamma_{B \rightarrow O} - (3/4)\Gamma_{O \rightarrow B} = 0$ or

$$\Gamma_{O \rightarrow B} = \Gamma_{B \rightarrow O}/3. \quad (63)$$

The numerical histograms of switching time distributions (see inset of Fig. 6), which were accumulated in a Monte-Carlo computation, confirm the long-time exponential decay of the “survival” probability $\rho_{11}^B(t)$ as well as the asymptotic rates (58), (61), and (63).

If a state’s lifetime in the oscillatory subspace, $\tau_O \equiv 1/\Gamma_{O \rightarrow B}$, is sufficiently long, it is possible to measure the spectrum described by Eq. (47). The necessary condition for this is $\tau_O \gtrsim \tau_{meas}$ where $\tau_{meas} \sim 1/\Gamma$ is a typical measurement time needed to achieve signal-to-noise ratio close to unity.²⁶ For small efficiency η we estimate (see Appendix B)

$$\tau_{meas} \simeq \frac{9}{32\Gamma\eta^2} \quad (64)$$

while for η close to unity the measurement time may become an order of magnitude larger than (64). Physically, the lifetime will satisfy $\tau_O \gtrsim \tau_{meas}$ if one can tune close to the symmetric point of identical qubits (small $\Delta\Omega$) and if the efficiency η is not too small.

The spectrum accumulated for times much greater than the lifetime τ_O gets averaged by switching events. Since the system resides in the spin-0 subspace 1/4 of the time and in the spin-1 subspace the remaining 3/4, the spectrum will take the form (47) with a factor of 2 instead of 8/3 (i.e. the peak-to-pedestal ratio will be 8η). There will be no additional peak at zero frequency because the averaged currents in the two scenarios coincide.

2. Purely quadratic detection

For a purely quadratic detector ($\delta = -2$) in the case of $\Gamma \gg \Delta\Omega \neq 0$, Eq. (53) produces switching transitions between states $|1\rangle^B$ and $|2\rangle^B$ while the oscillating state inside $\{|3\rangle^B, |4\rangle^B\}$ does not switch. The stationary solution to the master equation is similar to (38), but now $\rho_{11, st}^B = \rho_{22, st}^B = \frac{1}{2}[\rho_{11}^B(0) + \rho_{22}^B(0)]$. The new measurement subspaces are the minus subspace “−” = $\{|1\rangle^B, |2\rangle^B\}$ and the plus subspace “+” = $\{|3\rangle^B, |4\rangle^B\}$, where the names are based upon (10) - (13). The switching rates are given by

$$\Gamma_{|1\rangle^B \rightarrow |2\rangle^B} = \Gamma_{|2\rangle^B \rightarrow |1\rangle^B} = \frac{(\Delta\Omega)^2}{2\Gamma}, \quad (65)$$

derived by solving master equations to lowest order in $\Delta\Omega$ as in the derivation of Eq. (58). Switching between $|1\rangle^B$ and $|2\rangle^B$, and therefore between currents I_{23} and I_{14} in Fig. 2, produces telegraph noise.^{57,58} As a result, if we measure long enough ($t \gg 1/\Gamma_{|1\rangle^B \rightarrow |2\rangle^B}$), the power spectrum will exhibit a peak at zero frequency

$$S_I(\omega) = S_0 + \frac{(\Delta I)^2 \Gamma}{(\Delta\Omega)^2} \frac{1}{1 + [\omega\Gamma/(\Delta\Omega)^2]^2} \quad (66)$$

in full analogy with the one-qubit case.

Actually, it is possible to derive the power spectrum for arbitrarily large $\Delta\Omega$:

$$S_I(\omega) = S_0 + \frac{(\Delta\Omega)^2 (\Delta I)^2 \Gamma}{[\omega^2 - (\Delta\Omega)^2]^2 + \Gamma^2 \omega^2} \quad (67)$$

which reduces to (66) for small $\Delta\Omega$. Indeed, after collapse to the “−” or “+” subspaces, Eqs. (14), (15), (23), and (24) produce weakly perturbed quantum oscillations within the subspace and no switching to the other subspace. The quantum oscillations in the minus and plus subspaces correspond directly to one-qubit dynamics with oscillation frequency $\Delta\Omega$ and frequency $2\Omega \equiv (\Omega_a + \Omega_b)$ respectively. After a collapse in the “−” subspace the spectrum will be given by (67). If collapse has happened in the “+” subspace the spectrum will be given by Eq. (49) with a peak at 2Ω . In both cases the

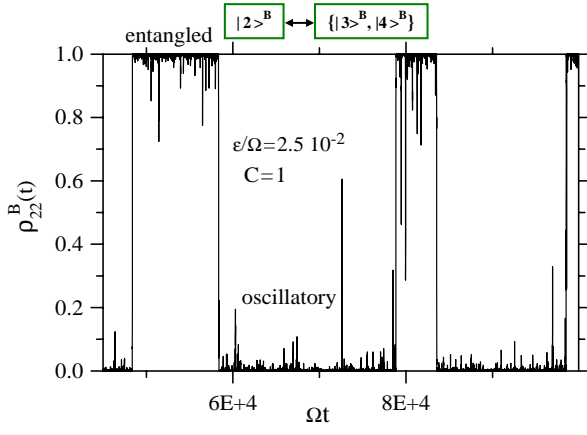


FIG. 7: *Quadratic detection.* Switching between Bell subspaces $|2\rangle^B$ and $\{|3\rangle^B, |4\rangle^B\}$ of Eqs. (10) – (13) as seen in the time evolution of $\rho_{22}^B(t)$, due to a small qubit bias. $|1\rangle^B$ is unaffected as seen from (29). The parameters are: $C = 1$, and $\varepsilon/\Omega \simeq 2.5 \times 10^{-2}$.

maximum peak-to-pedestal ratio at a non-zero frequency is 4η .

Measuring the spectrum on a sufficiently long time scale will constitute an (effective) measurement of the operator $\sigma_x^{(1)} \sigma_x^{(2)}$ whose eigenspaces are the “–” and “+” subspaces.

As we mentioned in Sec.III E, if instead of an asymmetry in frequency, the qubits are identical and biased $\varepsilon_a = \varepsilon_b = \varepsilon \ll \Gamma \ll \Omega$, under quadratic measurement switching will occur between the $|2\rangle^B$ state and the $\{|3\rangle^B, |4\rangle^B\}$ subspace (see Eq. (29)). The spin-0 subspace $|1\rangle^B$ will be unaffected as shown in Fig. 7.

The asymptotic switching rates (relevant at times $t \gtrsim 1/\Gamma$) are derived by study of master equations. The stationary solutions are given by (31) and the switching rate by

$$\Gamma_{|2\rangle^B \rightarrow \{|3\rangle^B, |4\rangle^B\}} = \frac{2\varepsilon^2}{\Omega^2} \Gamma. \quad (68)$$

Since $\rho_{22, st}^B = \rho_{33, st}^B = \rho_{44, st}^B = 1/3$, $\rho_{11, st}^B = \rho_{i \neq j, st}^B = 0$ is a stationary solution of the master equation within the spin-1 subspace, the stationary condition must be $(1/3)\Gamma_{|2\rangle^B \rightarrow \{|3\rangle^B, |4\rangle^B\}} - (2/3)\Gamma_{\{|3\rangle^B, |4\rangle^B\} \rightarrow |2\rangle^B} = 0$, implying

$$\Gamma_{\{|3\rangle^B, |4\rangle^B\} \rightarrow |2\rangle^B} = \frac{1}{2} \Gamma_{|2\rangle^B \rightarrow \{|3\rangle^B, |4\rangle^B\}}. \quad (69)$$

When the system collapses to $|1\rangle^B$, the power spectrum remains flat $S_I(\omega) = S_0$. In the case of switching between $|2\rangle^B$ and $\{|3\rangle^B, |4\rangle^B\}$, we can average the spectra as in the linear case above and add a telegraph noise peak caused by switching between current levels I_{14} and $(I_{23} + I_{14})/2$. The result is

$$S_I(\omega) = S_0 + \frac{2}{3} \frac{4\Omega^2 (\Delta I)^2 \Gamma}{(\omega^2 - 4\Omega^2)^2 + \Gamma^2 \omega^2}$$

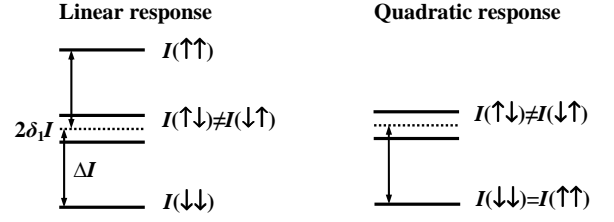


FIG. 8: Current levels for asymmetrically coupled qubits, $\Delta I_a \neq \Delta I_b$. Linear and quadratic response.

$$+ \frac{2(\Delta I)^2 \Omega^2}{27\varepsilon^2 \Gamma} \frac{1}{1 + [\omega \Omega^2 / 3\varepsilon^2 \Gamma]^2}. \quad (70)$$

Note that the peak-to-pedestal ratio at 2Ω is multiplied by a factor $2/3$ as a result of the averaging. This result can be reproduced also in the ensemble averaged approach.^{35,36}

To conclude this section we mention that a non-zero qubit interaction U does not mix the measurement subspaces, neither in the linear nor in the quadratic case. Correspondingly, calculations show that neither the stationary solutions of the master equations nor the switching rates derived above will be affected. Finite U will only affect the form of the spectrum in the oscillating scenario as described in Sec.III E.

B. Slightly different couplings

For identical qubits with slightly different coupling to the detector, $I_2 \neq I_3$ as indicated in Fig. 8. This asymmetry introduces evolution between collapse subspaces. The presence of the detector provides quantum Zeno stabilization, and so instead of gradual evolution, there is rare, abrupt switching between the subspaces. It is convenient to introduce the current asymmetry $\delta_1 I \equiv (I_2 - I_3)/2 = (\Delta I_a - \Delta I_b)/2$ and to define the current difference as $\Delta I = \Delta I_a - \delta_1 I = \Delta I_b + \delta_1 I = (\Delta I_a + \Delta I_b)/2$. The current asymmetry parameter is $\delta_1 \equiv \delta_1 I / \Delta I$. Defining the difference in coupling by $\Delta C = C_a - C_b$ and the average coupling by $C = (C_a + C_b)/2$, we note that in cases of small coupling asymmetry, $\delta_1 \simeq \frac{\Delta C}{4C}$.

1. Linear detection

If $\delta_1 \neq 0$, the following additional terms arise in the master equation in the case of linear detection

$$\left. \frac{d\rho_{ij}^B}{dt} \right|_{\text{meas, mix}} = \frac{(\Delta I)^2}{\eta 4 S_0} \left[2\delta_1 \begin{pmatrix} 0 & \rho_{34}^B & 0 & \rho_{32}^B \\ \cdot & 0 & \rho_{41}^B & 0 \\ \cdot & \cdot & 0 & \rho_{12}^B \\ \cdot & \cdot & \cdot & 0 \end{pmatrix} \right] \quad (71)$$

$$-2(\delta_1)^2 \begin{pmatrix} (\rho_{11}^B - \rho_{33}^B) \rho_{12}^B/2 & 2i\text{Im}\rho_{13}^B & \rho_{14}^B/2 \\ \cdot & \rho_{23}^B/2 & 0 \\ \cdot & \cdot & (\rho_{33}^B - \rho_{11}^B) \rho_{34}^B/2 \\ \cdot & \cdot & \cdot & 0 \end{pmatrix}$$

If the system starts in the entangled initial condition, $\rho_{11}^B = 1$, the exact solution to the master equation for small times is

$$\rho_{11}^B(t) = 1 - 2(\Gamma\delta_1^2)t + 4(\Gamma\delta_1^2)^2 t^2 + \dots \quad (72)$$

The solution contains a linear term setting a time scale $(\Gamma\delta_1^2)^{-1} \gg \Gamma^{-1}$. For $\rho_{11}^B(t)$ close to unity, the asymptotic rate of switching from the spin-0 Bell state $|1\rangle^B$ to the spin-1 subspace is found to be

$$\Gamma_{B \rightarrow O}^{C_a \neq C_b} = 2\Gamma\delta_1^2 = \frac{(I_2 - I_3)^2}{\eta 8S_0} \cong \frac{1}{8} \left(\frac{\Delta C}{C} \right)^2 \Gamma, \quad (73)$$

where the qubit detector couplings are slightly different, $\Delta I_a \neq \Delta I_b$. The reverse switching rate is given by Eq. (63).

To understand Eq. (73), we note that measurement for a short interval δt cannot distinguish between the current levels I_2 and I_3 when $(I_2 - I_3)^2 \ll D_I$ where $D_I = S_0/2\delta t$ is the variance of the measured noisy current. For a system initially in the spin-0 state $|1\rangle^B \sim |2\rangle - |3\rangle$ weak measurement tends to collapse the system towards either $|2\rangle$ or $|3\rangle$, thereby diminishing the amount of entangled state $|1\rangle^B$. Standard decoherence⁵⁵ in the measurement basis $\rho_{23} \rightarrow \rho_{23} \exp(-(I_2 - I_3)^2/8D_I)$ leads in the Bell basis to $\rho_{11}^B(t) \simeq 1 - [(I_2 - I_3)^2/8S_0] \delta t$ in agreement with (73). Note that the rate (73) is one half of the average classical information acquisition rate^{39,47} ($\Gamma_{cl} = (I_2 - I_3)^2/\eta 4S_0$) for a weakly measured fictitious two level system, as expected.

2. Quadratic detection

In the case of quadratic detection, if I_2 and I_3 are slightly different while I_1 remains equal to I_4 , then the two qubits have slightly different couplings and also the detector deviates slightly from being purely quadratic. The additional terms in the master equations take the form (71) but with the index ‘‘2’’ interchanged with the index ‘‘4’’ everywhere in the first matrix. As a result, the state $|2\rangle^B$ is unaffected, while rare switching develops between the state $|1\rangle^B$ and oscillations in the subspace $\{|3\rangle^B, |4\rangle^B\}$. The small time expansion of $\rho_{11}^B(t)$ takes the same form (72) and thus the rate $\Gamma_{|1\rangle^B \rightarrow \{|3\rangle^B, |4\rangle^B\}}$ is the same as in the linear case, Eq. (73):

$$\Gamma_{|1\rangle^B \rightarrow \{|3\rangle^B, |4\rangle^B\}} = \frac{\Gamma}{2} \left(\frac{I_2 - I_3}{\Delta I} \right)^2, \quad (74)$$

Since $\rho_{11, st}^B = \rho_{33, st}^B = \rho_{44, st}^B = 1/3$, $\rho_{i \neq j, st}^B = 0$ is a stationary solution to the master equation within the subspace $\{|1\rangle^B, |3\rangle^B, |4\rangle^B\}$, the reverse switching rate

is $\Gamma_{\{|3\rangle^B, |4\rangle^B\} \rightarrow |1\rangle^B} = \frac{1}{2} \Gamma_{|1\rangle^B \rightarrow \{|3\rangle^B, |4\rangle^B\}}$. In the case of collapse to $|2\rangle^B$, the spectrum remains flat, $S_I(\omega) = S_0$. Otherwise, for measurements over a time interval too short for switching, the system will reside in $|1\rangle^B$ leading to $S_I(\omega) = S_0$ or in the subspace $\{|3\rangle^B, |4\rangle^B\}$, leading to Eq. (49). For longer times, the spectrum will be the average of $S_I(\omega) = S_0$ and the spectrum given by Eq. (49) together with a telegraph noise peak:

$$S_I(\omega) = S_0 + \frac{2}{3} \frac{4\Omega^2(\Delta I)^2\Gamma}{(\omega^2 - 4\Omega^2)^2 + \Gamma^2\omega^2} + \frac{8(\Delta I)^4}{27\Gamma(I_2 - I_3)^2} \frac{1}{1 + [4\omega(\Delta I)^2/3\Gamma(I_2 - I_3)^2]^2}. \quad (75)$$

The peak-to-pedestal ratio at 2Ω will be $(8/3)\eta$ rather than 4η as a result of the averaging.

If the detector has $I_1 \neq I_4$ while $I_2 = I_3$, switching occurs between the state $|2\rangle^B$ and the oscillating subspace $\{|3\rangle^B, |4\rangle^B\}$, while state $|1\rangle^B$ is unaffected (as in Fig.7). This slightly non-quadratic mode of detection is ‘‘orthogonal’’ to the $I_2 \neq I_3$ mode in the sense that the switching rate would not depend on a small additional $I_2 \neq I_3$ - asymmetry. The rates are

$$\Gamma_{|2\rangle^B \rightarrow \{|3\rangle^B, |4\rangle^B\}} = \frac{\Gamma}{2} \left(\frac{I_1 - I_4}{\Delta I} \right)^2, \quad (76)$$

$$\Gamma_{\{|3\rangle^B, |4\rangle^B\} \rightarrow |2\rangle^B} = \frac{1}{2} \Gamma_{|2\rangle^B \rightarrow \{|3\rangle^B, |4\rangle^B\}}. \quad (77)$$

The power spectrum for large times will be given by Eq. (75) with the substitution $(I_2 - I_3) \rightarrow (I_1 - I_4)$.

When $I_2 \neq I_3$ and $I_1 \neq I_4$, we combine the two cases $I_2 \neq I_3$, $I_1 = I_4$ and $I_2 = I_3$, $I_1 \neq I_4$. Based on the analysis above, there should be switching $|1\rangle^B \leftrightarrow \{|3\rangle^B, |4\rangle^B\} \leftrightarrow |2\rangle^B$ but no direct switching between $|1\rangle^B$ and $|2\rangle^B$. The stationary solution of the master equation is $\rho_{ii, st}^B = 1/4$, $\rho_{i \neq j, st}^B = 0$, so only one half of the time is spent in the oscillatory state, and therefore the peak-to-pedestal ratio at 2Ω is 2η rather than 4η . The current spectral density in this case, including a low-frequency peak due to telegraph noise in a 3-terminal system, is

$$S_I(\omega) = S_0 + \frac{1}{2} \frac{4\Omega^2(\Delta I)^2\Gamma}{(\omega^2 - 4\Omega^2)^2 + \Gamma^2\omega^2} + \frac{(\Delta I)^2(\Gamma_1 + \Gamma_2)(4\Gamma_1\Gamma_2 + \omega^2)}{16\Gamma_1^2\Gamma_2^2 + (9\Gamma_1^2 + 2\Gamma_1\Gamma_2 + 9\Gamma_2^2)\omega^2 + 4\omega^4} \quad (78)$$

where $\Gamma_1 \equiv \Gamma_{|1\rangle^B \rightarrow \{|3\rangle^B, |4\rangle^B\}}$ and $\Gamma_2 \equiv \Gamma_{|2\rangle^B \rightarrow \{|3\rangle^B, |4\rangle^B\}}$ are given by (74) and (76).

C. Environmental dephasing

We have studied the effect of environmental dephasing, modeling it with two small dephasing rates γ_a and γ_b acting separately on the qubits. This adds an extra dephasing contribution $\tilde{\gamma}_{ij}$ to γ_{ij} in Bayesian equation

(6) where

$$\tilde{\gamma}_{ij} = \begin{pmatrix} 0 & \gamma_b & \gamma_a & \gamma_a + \gamma_b \\ \gamma_b & 0 & \gamma_a + \gamma_b & \gamma_a \\ \gamma_a & \gamma_a + \gamma_b & 0 & \gamma_b \\ \gamma_a + \gamma_b & \gamma_a & \gamma_b & 0 \end{pmatrix}. \quad (79)$$

We assume that the coupling to the environment is much smaller than the coupling to the detector, $\gamma_a, \gamma_b \ll \Gamma$. Numerical simulation again shows that abrupt switching events take place. However, now the density matrix ρ remains slightly mixed even for an ideal detector.

In the linear case we have switching between spin-0 and spin-1 subspaces. Analyzing the resulting master equations, we derive in the case of a linear detector the switching rates

$$\Gamma_{B \rightarrow O}^{\gamma_a, \gamma_b} = 3\Gamma_{O \rightarrow B}^{\gamma_a, \gamma_b} = (\gamma_a + \gamma_b)/2. \quad (80)$$

In the quadratic case the switching involves transitions $|1\rangle^B \leftrightarrow \{|3\rangle^B, |4\rangle^B\} \leftrightarrow |2\rangle^B$, with again no direct switching between $|1\rangle^B$ and $|2\rangle^B$. The rates are $\Gamma_{|1\rangle^B \rightarrow \{|3\rangle^B, |4\rangle^B\}} = \Gamma_{|2\rangle^B \rightarrow \{|3\rangle^B, |4\rangle^B\}} = (\gamma_a + \gamma_b)/2$, and the reverse switching rates follow from the stationary state.

V. CONCLUSION

In this paper we have investigated in detail the non-trivial interplay between the internal two-qubit Hamiltonian evolution and two-qubit dynamics under weak continuous measurement described by a Bayesian formalism. The gradual collapse of the system's quantum state takes a finite measurement time $\tau_{meas} \sim 1/\Gamma$. On a time scale greater than $1/\Gamma$, the measurement effectively looks like orthodox projective measurement in the Bell basis. A linear or non-linear detector measures the operator of total "spin", $(\vec{\sigma}^{(1)} + \vec{\sigma}^{(2)})^2$. The system's possible collapse subspaces are the spin-0 Bell state, $|1\rangle^B$ and the spin-1 subspace within which the system executes oscillations. For purely quadratic measurement, the operator $\sigma_y^{(1)} \sigma_y^{(2)} + \sigma_z^{(1)} \sigma_z^{(2)}$ is measured so that the collapse subspaces are the spin-0 state, the other Bell state, $|2\rangle^B$, and the oscillation subspace $\{|3\rangle^B, |4\rangle^B\}$.

Measurement leads to spontaneous entanglement which can be identified by a distinct power spectrum and/or distinct value of the average current of the detector. We obtained analytically the power spectrum of the current, $S_I(\omega)$, in different situations. In particular, in the case of a linear (purely quadratic) detector response for non-interacting identical qubits the spectrum exhibits a Lorentzian single peak at frequency Ω (2Ω) with peak-to-pedestal ratio of $(32/3)\eta$ (4η) respectively. We also obtained analytic expressions in the case of qubit biasing and in the presence of qubit-qubit interaction. For a general non-linear measurement the spectrum can be calculated using numerical simulations of the measurement process.

Various small imperfections of the two-qubit system such as asymmetry of the Hamiltonian and/or asymmetry in the coupling to detector cause transitions between collapsed states. Because the coupling to the detector, although weak compared to most of the energy scales in the Hamiltonian, can be strong compared to the small imperfection, a regime of quantum Zeno-like stabilization arises. The system does not drift gradually from one collapse subspace to another; instead it remains stabilized in one subspace and experiences rare, abrupt switching events to other subspaces. For very long observational times, because of the switching, one observes only averaged dynamics in the power spectrum.

The authors gratefully acknowledge the support of the Packard foundation (R.R. and A.M.) and of NSA and ARDA under ARO grant W911NF-04-1-0204 (A.K.).

APPENDIX A: CALCULATION OF THE STATIONARY DISTRIBUTION FOR ρ_{22}^B

In this Appendix, we use a Fokker-Plank equation to calculate the stationary distribution for ρ_{22}^B and its moments in the case of linear detection in the oscillating scenario of Fig. 5 and Eqs. (34)–(37).

An Itô stochastic equation for ρ_{22}^B can be derived from Eqs. (23)–(28), and the parameterizations (34)–(37), that depends only on the two independent variables, $x(t) \equiv \rho_{22}^B(t)$ and $\varphi(t)$:

$$\frac{dx}{dt} = 2 \frac{\Delta I}{S_0} \sqrt{x(1-x)} (1-2x) \cos(\Omega t + \varphi(t)) \xi(t) - 2\Gamma [x - (1-x) \cos^2(\Omega t + \varphi(t))]. \quad (A1)$$

In the weak coupling regime one can average over the oscillations with frequency Ω . Then $\langle \cos^2(\Omega t + \varphi(t)) \rangle \rightarrow 1/2$ and

$$\frac{dx}{dt} = \frac{\Delta I}{S_0} \sqrt{2x(1-x)} (1-2x) \xi_1(t) - \Gamma (3x - 1), \quad (A2)$$

where, $\xi_1(t)$ is an effective white noise with the same spectral density.

A Fokker-Plank equation for the distribution $P(x, t)$ follows^{56,57} from Eq. (A2)

$$\frac{\partial P(x, t)}{\partial t} = -\frac{\partial}{\partial x} [B(x)P(x, t)] + \frac{S_0}{4} \frac{\partial^2}{\partial x^2} [C^2(x)P(x, t)] \quad (A3)$$

with $B(x) \equiv -\Gamma(3x - 1)$ and $C(x) \equiv \frac{\Delta I}{S_0} \sqrt{2x(1-x)}$. A stationary solution of Eq. (A3) can be derived⁵⁶ taking into account that $x = \rho_{22}^B$ is a restricted variable and therefore the "probability current flow" is zero.

$$P(x) = N_0^{-1} \frac{\exp\left[-\frac{1}{2(1-2x)}\right]}{x^{1/2}(1-2x)^{7/2}} \quad (A4)$$

with normalization constant $N_0 = 6\sqrt{\pi/e}$. Eq. (A4) implies that ρ_{22}^B actually fluctuates between 0 and $1/2$,

which is confirmed by Monte-Carlo simulations, Fig. 5. For the moments, $\langle x^n \rangle \equiv \int_0^{1/2} x^n P(x) dx$, one obtains

$$\langle x \rangle = 1/3, \quad \langle x^2 \rangle = 1/8, \quad \dots \quad (\text{A5})$$

$$\langle x^n \rangle = (N_0)^{-1} \left[3\sqrt{2\pi} {}_1F_1\left(\frac{1}{2} - n, -\frac{3}{2}; -\frac{1}{2}\right) - \frac{8\sqrt{\pi}}{15} \frac{\Gamma(n + \frac{1}{2})}{\Gamma(n - 2)} {}_1F_1\left(3 - n, \frac{7}{2}; -\frac{1}{2}\right) \right] 2^{1/2-n} \quad (\text{A6})$$

where ${}_1F_1(a, b; z)$ is the confluent hypergeometric function.

APPENDIX B: NOISE OF THE NOISE AND THE MEASUREMENT TIME TO ACCUMULATE THE SPECTRUM

Here we calculate the measurement time to distinguish between a flat spectrum (shot noise) and a spectrum that possesses a peak on the top of the shot noise pedestal. To make an estimation we first consider a situation with a narrow band ($\Delta f \ll f$, $f \equiv \omega/2\pi$) frequency filter. The average power for a finite time Δt ($\geq 1/\Delta f$) is a fluctuating quantity, $\mathcal{P} = \frac{1}{\Delta t} \int_{-\frac{\Delta t}{2}}^{\frac{\Delta t}{2}} dt (I(t) - I_0)^2$, that depends on Δt and on realizations of the process. Denoting the fluctuating part of the current as $\tilde{I}(t) \equiv I(t) - I_0$ we perform averaging over realizations using the well known relation to the noise power spectrum (see, e.g. Ref. 57): $\langle \tilde{I}^2(t) \rangle_r \simeq S_I(\omega)\Delta f$. Therefore, averaging of \mathcal{P} gives

$$\langle \mathcal{P} \rangle_r = \left\langle \frac{1}{\Delta t} \int_{-\frac{\Delta t}{2}}^{\frac{\Delta t}{2}} dt (I(t) - I_0)^2 \right\rangle_r \simeq S_I(\omega)\Delta f. \quad (\text{B1})$$

The second moment, $\langle \mathcal{P}^2 \rangle_r$, can be evaluated for a Gaussian random process $I(t)$, using stationarity:

$$\begin{aligned} \langle \mathcal{P}^2 \rangle_r &= \left\langle \left[\frac{1}{\Delta t} \int_{-\frac{\Delta t}{2}}^{\frac{\Delta t}{2}} dt (I(t) - I_0)^2 \right]^2 \right\rangle_r \\ &\simeq \frac{1}{\Delta t} \int_{-\infty}^{\infty} d\tau K_{I^2}(\tau) + (S_I(\omega)\Delta f)^2, \end{aligned} \quad (\text{B2})$$

where $K_{I^2}(\tau)$ is the correlation function of the ‘‘power signal’’ $\tilde{I}^2(t) - \langle \tilde{I}^2(t) \rangle_r$

$$K_{I^2}(\tau) \equiv \left\langle \left[\tilde{I}^2(t) - \langle \tilde{I}^2 \rangle_r \right] \left[\tilde{I}^2(t + \tau) - \langle \tilde{I}^2 \rangle_r \right] \right\rangle_r. \quad (\text{B3})$$

The variance of the fluctuating power, Eq.(B2), is expressed through the ‘‘second’’ spectral density $S_{I^2}(\omega) \equiv$

$2 \int_{-\infty}^{\infty} d\tau K_{I^2}(\tau) e^{i\omega\tau}$, which for a Gaussian process $I(t)$ is related to the ordinary one.⁵⁷ In particular, $S_{I^2}(0) = 2[S_I(\omega)]^2\Delta f$ and we obtain

$$\Delta \mathcal{P}^2 \equiv \langle \mathcal{P}^2 \rangle_r - \langle \mathcal{P} \rangle_r^2 = \frac{1}{\Delta t} [S_I(\omega)]^2 \Delta f. \quad (\text{B4})$$

For a more general frequency filter $\alpha(f)$ the power is distributed with average and variance respectively given as $\langle \mathcal{P} \rangle_r = \int_0^\infty \alpha(f) S_I(\omega) df$ and $\Delta \mathcal{P}^2 = \frac{1}{\Delta t} \int_0^\infty \alpha^2(f) [S_I(\omega)]^2 df$ that generalize Eqs.(B1),(B4).

We are interested in measuring $I(t)$ to distinguish between two hypotheses: (1) flat power spectrum $S_I(\omega) = S_0$ and (2) power spectrum with a peak $S_I(\omega) = S_0 + S_{peak}(f)$. Assuming Gaussian distribution of the power signal we can estimate the measurement time τ_{meas} at which the variances $\Delta \mathcal{P}_1^2[\alpha(f)]$, $\Delta \mathcal{P}_2^2[\alpha(f)]$, become small enough to distinguish between the corresponding averages $\langle \mathcal{P}_1 \rangle_r$, $\langle \mathcal{P}_2 \rangle_r$. For a ‘‘signal-to-noise’’ ratio of 1, τ_{meas} is expressed as (see also Ref.26)

$$\tau_{meas} = \frac{\left[\sqrt{\Delta \mathcal{P}_1^2[\alpha(f)]} + \sqrt{\Delta \mathcal{P}_2^2[\alpha(f)]} \right]^2}{\left[\int_0^\infty \alpha(f) S_{peak}(f) df \right]^2}. \quad (\text{B5})$$

Optimization over the filter requires $\delta\tau_{meas}/\delta\alpha(f) = 0$, which leads to the filter form

$$\alpha(f) = \frac{S_{peak}(f)}{1 + a(1 + S_{peak}(f)/S_0)^2} \quad (\text{B6})$$

that is close to the peak form itself while further optimization on the parameter a is needed. However, for a small peak height, $h \approx S_{peak}(\Omega)/S_0 \ll 1$, the result is independent of a and reads

$$\tau_{meas} = \frac{32}{\Gamma h^2}. \quad (\text{B7})$$

Note that small height translates to small detector ideality (for one qubit $h \leq 4\eta$ while for two qubits $h \leq 32\eta/3$). To get an exact result for large or small height, one employs integration by residues and find a cumbersome expression that can only be managed numerically. Numerically, the calculation suggests that a_{opt} is of the order of 1. An approximation with accuracy better than 30% even at large η is given by

$$\tau_{meas} = \frac{32}{\Gamma h^2} \left(1 + \frac{3h}{4} + \frac{7h^2}{64} \right) \quad (\text{B8})$$

which means that τ_{meas} may become an order of magnitude larger than the simple estimate, Eq.(B7).

¹ V. B. Braginsky and F. Ya. Khalili, *Quantum measurement* (Cambridge Univ. Press, Cambridge, UK, 1992).

² E. Joos, H.D. Zeh, C. Kiefer, D. Giulini, J. Kupsch, and

I.-O. Stamatescu, *Decoherence and appearance of classical world in quantum theory*, (Springer, Heidelberg, 2003).

³ M. Namiki, S. Pascazio, and H. Nakazato, *Decoherence*

- and *Quantum measurements*, (World Scientific, Singapore, 1997).
- ⁴ L.S. Khal'fin, JETP Lett. **8**, 63 (1968).
 - ⁵ B. Misra and E. C. G. Sudarshan, J. Math. Phys. **18**, 756 (1977); C.B Chiu, E. C. G. Sudarshan, and B. Misra, Phys. Rev. D **16**, 520 (1977).
 - ⁶ A. Peres, Am. J. Phys. **48**, 931 (1980).
 - ⁷ E. Joos, Phys. Rev. D **29**, 1626 (1984).
 - ⁸ R. J. Cook, Phys. Scr. T **21**, 49 (1988); G. J. Milburn, J. Opt. Soc. Am. B **5**, 1317 (1988); A. Beige and G. C. Hegerfeldt, J. Phys. A **40**, 1323 (1997); L. S. Schulman, Phys. Rev. A **57**, 1509 (1998); A. G. Kofman and G. Kurizki, Nature **405**, 546 (2000); P. Facchi, H. Nakazato, S. Pascazio, Phys. Rev. Lett. **86**, 2699 (2001).
 - ⁹ An alternative mechanism for stabilization of a quantum state is provided by a strong coupling to a noisy environment¹⁰. Suppression of the quantum transition in a two-level macroscopic quantum system due to large dissipation is discussed, e.g., in Ref.11.
 - ¹⁰ M. Simonius, Phys. Rev. Lett. **40**, 980 (1978); R.A. Harris and L. Stodolsky, Phys. Lett. B **116**, 464 (1982); Ph. Blanchard, G. Bolz, M. Cini, G.F. De Angelis, and M. Serva, J. of Stat. Phys., **75**, 749 (1994).
 - ¹¹ A. J. Leggett in *Directions in Condensed Matter Physics*, eds. G. Grinstein and G. Mazenko, (World Scientific, Singapore, 1986).
 - ¹² W. M. Itano, D. J. Heinzen, J. J. Bollinger, and D. J. Wineland, Phys. Rev. A **41**, 2295 (1990).
 - ¹³ M. C. Fischer, B. Gutiérrez-Medina, and M.G. Raizen, Phys. Rev. Lett. **87**, 040402 (2001).
 - ¹⁴ Y. Nakamura, Yu. A. Pashkin, and J. S. Tsai, Nature (London) **398**, 786 (1999); C. H. van der Wal, A.C.J. ter Haar, F. K. Wilhelm, R. N. Schouten, C.J.P.M. Harmans, T. P. Orlando, S. Lloyd, and J. E. Mooij, Science **290**, 773 (2000); J. R. Friedman, V. Patel, W. Chen, S. K. Tolpygo, and J. E. Lukens, Nature (London) **406**, 43 (2000); D. Vion, A. Aassime, A. Cottet, P. Joyez, H. Pothier, C. Urbina, D. Esteve, and M. H. Devoret, Science **296**, 886 (2002); J. M. Martinis, S. Nam, J. Aumentado, and C. Urbina, Phys. Rev. Lett. **89**, 117901 (2002).
 - ¹⁵ E. Buks, R. Schuster, M. Heiblum, D. Mahalu, and V. Umansky, Nature **391**, 871 (1998); T. Hayashi, T. Fujisawa, H. D. Cheong, Y. H. Jeong, and Y. Hirayama, Phys. Rev. Lett. **91**, 226804 (2003); W. Lu, Z. Ji, L. Pfeifer, K. W. West, and A. J. Rimberg, Nature **423**, 422 (2003); N. J. Graig, J. M. Taylor, E. A. Lester, C. M. Marcus, M. P. Hanson, and A. C. Gossard, Science **304**, 565 (2004).
 - ¹⁶ D. V. Averin, Fortschr. Phys. **48**, 1055 (2000).
 - ¹⁷ M. H. Devoret and R. Schoelkopf, Nature **406**, 1039 (2000); T. Duty, D. Gunnarsson, K. Bladh, and P. Delsing, Phys. Rev. B **69**, 140503(R) (2004); A. Guillaume, J. F. Schneiderman, P. Delsing, H. M. Bozler, and P. M. Echternach, Phys. Rev. B **69**, 132504 (2004).
 - ¹⁸ E. Il'ichev, N. Oukhanski, A. Izmalkov, Th. Wagner, M. Grajcar, H.-G. Meyer, A.Yu. Smirnov, Alec Maassen van den Brink, M.H.S. Amin, and A.M. Zagoskin, Phys. Rev. Lett. **91**, 097906 (2003).
 - ¹⁹ J. von Neumann, *Mathematical Foundations of Quantum Mechanics* (Princeton Univ. Press, Princeton, 1955).
 - ²⁰ M. B. Mensky, Phys. Rev. D **20**, 384 (1979).
 - ²¹ N. Gisin, Phys. Rev. Lett. **52**, 1657 (1984).
 - ²² C. M. Caves, Phys. Rev. D **33**, 1643 (1986).
 - ²³ H. J. Carmichael, *An open system approach to quantum optics*, Lecture notes in physics (Springer, Berlin, 1993).
 - ²⁴ M. B. Plenio and P. L. Knight, Rev. Mod. Phys. **70**, 101 (1998).
 - ²⁵ H. M. Wiseman and G. J. Milburn, Phys. Rev. Lett. **70**, 548 (1993); Phys. Rev. A **49**, 1350 (1994).
 - ²⁶ A. N. Korotkov, Phys. Rev. B **60**, 5737 (1999); Phys. Rev. B **63**, 115403 (2001).
 - ²⁷ A. N. Korotkov, cond-mat/0209629, in *Quantum noise in mesoscopic physics*, edited by Yu. V. Nazarov (Kluwer, Netherlands, 2003), p. 205.
 - ²⁸ H.-S. Goan, G. J. Milburn, H. M. Wiseman, and H. B. Sun, Phys. Rev. B **63**, 125326 (2001).
 - ²⁹ H.-S. Goan and G. J. Milburn, Phys. Rev. B **64**, 235307 (2001); N. P. Oxtoby, H. B. Sun, and H. M. Wiseman, J. Phys.: Condens. Matter **15**, 8055 (2003).
 - ³⁰ A. N. Korotkov and D. V. Averin, Phys. Rev. B **64**, 165310 (2001); A. N. Korotkov, Phys. Rev. B **63**, 085312 (2001).
 - ³¹ Yu. Makhlin, G. Schön, A. Shnirman, Phys. Rev. Lett. **85**, 4578 (2000).
 - ³² J. W. Lee, D. V. Averin, G. Benenti, and D. Shepelyansky, Phys. Rev. A **72**, 012310 (2005).
 - ³³ R. Ruskov, A. N. Korotkov, and A. Mizel, quant-ph/0505094.
 - ³⁴ R. Ruskov and A. N. Korotkov, Phys. Rev. B **67**, 241305(R) (2003).
 - ³⁵ W. Mao, D.V. Averin, R. Ruskov, and A. N. Korotkov, Phys. Rev. Lett. **93**, 056803 (2004).
 - ³⁶ W. Mao, D. V. Averin, F. Plastina, and R. Fazio, Phys. Rev. B **71**, 085320 (2005).
 - ³⁷ S. A. Gurvitz, Phys. Rev. B **56**, 15215 (1997).
 - ³⁸ D. V. Averin and R. Fazio, JETP Letter, **78**, 1162 (2003).
 - ³⁹ A. N. Korotkov, Phys. Rev. A **65**, 052304 (2002).
 - ⁴⁰ A. N. Korotkov, Phys. Rev. B **67**, 235408, (2003).
 - ⁴¹ R. Ruskov, K. Schwab, and A. N. Korotkov, Phys. Rev. B **71**, 235407, (2005).
 - ⁴² D. V. Averin and E. V. Sukhorukov, Phys. Rev. Lett. **95**, 126803 (2005).
 - ⁴³ B.Øksendal, *Stochastic differential equations* (Springer, Berlin, 1998).
 - ⁴⁴ C. W. Gardiner and P. Zoller, *Quantum noise* (Springer, Berlin, 2000).
 - ⁴⁵ A. O. Caldeira and A. J. Leggett, *Ann. Phys. (N.Y.)* **149**, 374 (1983); W. H. Zurek, *Physics Today* **44**, 36 (1991).
 - ⁴⁶ S. Pilgram and M. Büttiker, Phys. Rev. Lett. **89**, 200401 (2002).
 - ⁴⁷ A. A. Clerk, S. M. Girvin, and A. D. Stone, Phys. Rev. B **67**, 165324 (2003).
 - ⁴⁸ R. Ruskov and A. N. Korotkov, Phys. Rev. B **67**, 075303 (2003).
 - ⁴⁹ Experimentally¹⁵ QPC is close to an ideal detector. An SET is usually highly non-ideal²⁶, however it may reach ideality close to 1 in the co-tunneling or Cooper pair tunneling regime⁵⁰.
 - ⁵⁰ A. B. Zorin, Phys. Rev. Lett. **76**, 4408 (1996); D. V. Averin, cond-mat/0010052 (unpublished); A. A. Clerk, S. M. Girvin, A. K. Nguyen, and A. D. Stone, Phys. Rev. Lett. **89**, 176804 (2002).
 - ⁵¹ H. Mabuchi, H. M. Wiseman, Phys. Rev. Lett. **81**, 4620 (1998); Erratum-ibid. **82**, 1798 (1999).
 - ⁵² We also checked by numerical simulations of the measurement process that two observers, who start with different initial knowledge about the system (i.e., different initial density matrices $\rho_{ij}(0)$) will agree with each other about the state evolution after such measurement time (compare with Ref.41).

- ⁵³ L. N. Bulaevskii and G. Ortiz, Phys. Rev. Lett. **90**, 040401 (2003).
- ⁵⁴ A. Shnirman, D. Mozyrsky, and I. Martin, Europhys. Lett., **67** (5), 840 (2004).
- ⁵⁵ E. B. Davies, *Quantum Theory of Open Systems*, (Academic, London, 1976).
- ⁵⁶ C. W. Gardiner, *Handbook of Stochastic methods* (Springer, Berlin, 1983).
- ⁵⁷ Sh. Kogan, *Electronic noise and fluctuations in solids* (Cambridge University Press, Cambridge, USA, 1996).
- ⁵⁸ S. Machlup, J. Appl. Phys. **25**, 341 (1954).